Ridenour, N. A., Hu, X., Jafarikhasragh, S., Landy, J. C., Lukovich, J. V., Stadnyk, T. A., Sydor, K., Myers, P. G., & Barber, D. G. (2019). Sensitivity of freshwater dynamics to ocean model resolution and river discharge forcing in the Hudson Bay Complex. *Journal of Marine Systems*, *196*, 48-64. https://doi.org/10.1016/j.jmarsys.2019.04.002

Sensitivity of freshwater dynamics to ocean model resolution and river discharge forcing in the Hudson Bay Complex

Natasha A. Ridenour[a,*], Xianmin Hu[a,1], Shabnam JarfariKhasragh[b], Jack C. Landy[c], Jennifer V. Lukovich[b], Tricia A. Stadnyk[d], Kevin Sydor[e], Paul G. Myers[a], David G. Barber[b]

[a]*Department of Earth and Atmospheric Sciences, University of Alberta, Edmonton, Alberta, Canada*
[b]*Center for Earth Observation Science, University of Manitoba, Winnipeg, Manitoba, Canada*
[c]*Bristol Glaciology Centre, School of Geographical Sciences, University of Bristol, Bristol, United Kingdom*
[d]*Department of Civil Engineering (Water Resources), University of Manitoba, Winnipeg, Manitoba, Canada*
[e]*Manitoba Hydro, Winnipeg, Manitoba, Canada*

Abstract

Hydroelectric development and regulation have modified the temporal and spatial distribution of runoff entering the Hudson Bay Complex (HBC), which is the drainage basin for about 40% of Canada. To understand the impacts and future of regulation in this region, the numerical ocean model, NEMO, run with the Arctic and Northern Hemispheric Atlantic (ANHA) configuration, is used to model present day freshwater dynamics associated with river runoff and sea ice melt. The present work establishes the freshwater budget in each subregion of the HBC, in addition to evaluating the sensitivity to

*Corresponding author
Email address: ridenour@ualberta.ca (Natasha A. Ridenour)
[1]Now at Bedford Institute of Oceanography, Dartmouth, Nova Scotia, Canada

model resolution and estimates of river discharge forcing. It is shown that the annually averaged HBC freshwater budget is mainly a balance between river discharge and freshwater advected out of the region, while surface fluxes (ice melt and growth, and precipitation and evaporation) are the dominant term on seasonal time scales. Runoff forcing is found to impact the long term mean volume and freshwater fluxes out of the HBC, while increased resolution has minimal effect on these fluxes, with the exception of the Southampton–Baffin Island gate. Quantitative estimates of turbulent, mean, and Ekman components of freshwater exchange between the interior and boundary regions of Hudson Bay are also presented. We use offline Lagrangian passive tracers to estimate the HBC runoff residence time, which is as long as 21 years.
Keywords: Hudson Bay Complex, River runoff, Freshwater, dynamics, ocean modelling

1. Introduction

Anthropogenic changes such as global warming, which is causing an intensification of the hydrological cycle in the Arctic region (Zhang et al., 2012; Déry et al., 2009), as well as hydroelectric development, such as dams, reservoirs, and river diversions, are changing the river discharge in northern Canada (Déry et al., 2011, 2016; MacDonald et al., 2018; Déry et al., 2018). One such region undergoing these changes is the Hudson Bay Complex (HBC), which includes Hudson Bay, James Bay, and neighbouring basins, Foxe Basin, and Hudson Strait and Ungava Bay, shown in Figure 1. The HBC receives about 900 km^3/year of river runoff, equivalent to roughly three times the Mackenzie River (Shiklomanov and Shiklomanov, 2003; Holmes

et al., 2012), causing this region to be quite fresh compared to the Arctic Ocean. This river water flows out of Hudson Strait and along the coast of Labrador in the Labrador Sea, which is a key location for deep convection as part of the meridional overturning circulation, regulating the global climate (Aagaard and Carmack, 1989; Straneo, 2006; Lazier et al., 2002). Presently, the amount of Hudson Strait outflow mixed into the Labrador Sea interior is unknown, as low salinity water can increase stratification, potentially slowing down convection in this region.

Not only is it important to know the freshwater and volume fluxes entering the Labrador Sea from Hudson Strait, but also to know how freshwater and volume are exchanged within the HBC. Freshwater-marine coupling not only impacts the ocean and sea ice dynamics and thermodynamics, but also the biology and biogeochemistry of the bay. With future hydroelectric development in the bay, it is unclear the impacts changes in river discharge might have on the systems in the HBC. To remedy this gap in knowledge, a multidisciplinary project, known as BaySys, was formed. The objective of the project is to evaluate the impacts of the hydroelectric industry and climate change on the HBC.

The HBC is isolated from large scale ocean circulation, thus river discharge and sea ice melt are the two main sources of freshwater in the freshwater budget (Prinsenberg, 1988). On time scales less than a year, sea ice melt/growth has a much larger role in the freshwater budget compared to river discharge (Prinsenberg, 1988).

Chemical tracers have been used to determine the sources of freshwater in Hudson Bay and have shown that lower salinity water along the coast had

primarily freshwater from river discharge, while freshwater from sea ice melt was distributed more equally around the bay, with higher concentrations in the south due to the southward drift of sea ice during the melt season, as well as the presence of thicker ice at the end of spring (Granskog et al., 2007, 2011). Riverine water has been found throughout the water column in southeastern Hudson Bay, near James Bay, while along the northeastern coast of Hudson Bay, river water was mostly found in the top 50 m. Additionally, riverine water has been detected in lower concentrations at depth in the interior as well, due to dense water formation, allowing river water to mix down to deeper depths (Granskog et al., 2011).

Within Hudson Bay, Ekman transport is the main process exchanging freshwater between the interior and boundary regions of the bay, with an import of freshwater to the interior in summer, and release of this freshwater in the fall (St-Laurent et al., 2011, 2012).

In the context of climate change, many studies focus on the response of sea ice and its influence on the local ecosystem. The length of the ice free season is increasing, with both earlier break up in spring (Gough et al., 2004a; Gagnon and Gough, 2005; Castro de la Guardia et al., 2017; Hochheim and Barber, 2014; Kowal et al., 2017) and later freeze up in the fall (Gagnon and Gough, 2005; Castro de la Guardia et al., 2017; Hochheim and Barber, 2014; Kowal et al., 2017). These changes have been found to be related to the region's air temperature (Hochheim and Barber, 2010, 2014; McGovern and Gough, 2015). Quantitatively, for every 1°C increase in the region's mean air temperature, there is a decrease of 105,000–117,000 km^2 in late November sea ice extent with concentration greater than 80% (Hochheim

and Barber, 2010). As sea ice is essential to polar bear habitat, the changes in the ice free season may significantly impact the polar bear population in this region. Based on coupled sea ice–ocean model simulations, Castro de la Guardia et al. (2013) found that the ice free season increases by 1.7, 6.1, and 13.0 days per decade in the 21st century with three (low, medium, and high) greenhouse gas emission scenarios, thus they warned that the western Hudson Bay polar bear population will be threatened after 2060 for the medium and high emission scenarios due to sea ice loss.

Sea ice thickness, on the other hand, is weakly related to air temperatures, but snow depth has a leading role in the variability of ice thickness in the HBC, with the exception of Hall Beach (Gough et al., 2004b). However, until recently, sea ice thickness measurements in the HBC were challenging to obtain, and lacked high spatial resolution. Landy et al. (2017) presented the first high resolution ice thickness measurements for the HBC and eastern Canadian Arctic, derived from satellite altimetry. On average sea ice in Hudson Bay grows at a rate of 28 cm/month between November and April; however, by spring the ice thickness can be significantly asymmetrical across the bay after winters of strong cyclonic ice drift. From the high spatial resolution of measurements, this study was able to determine that 742 km^3 of freshwater is stored within the Hudson Bay sea ice cover in April. This volume varies by $\pm$14% between years owing to interannual variations in spring ice thickness.

Anthropogenic influences have also impacted the HBC river discharge. Discharge entering the HBC has increased (Déry et al., 2016), despite a negative trend observed in the second half of the 20th century (Shiklomanov

and Shiklomanov, 2003; Déry and Wood, 2004; Déry et al., 2005; McClelland et al., 2006). This increase is thought to be due to an intensifying hydrological cycle expected to accompany increased temperatures in the Arctic (Déry et al., 2011, 2016, 2009; Zhang et al., 2012; Rawlins et al., 2010). Seasonally, there has been an increase in HBC stream flow during winter due to hydroelectric development (Déry et al., 2011). Peak runoff in the spring has been occurring earlier in the year (Déry et al., 2005; Gagnon and Gough, 2002), due to increasing temperatures. However, regionally, in northern Hudson Bay, increased flow in the Kazan River (Figure 1) can be explained by higher year round precipitation, while in the south, there has been decreased flow in both the Grand Baleine River and Gods River (Gagnon and Gough, 2002). A recent study by MacDonald et al. (2018) used a hydrological model to investigate HBC river discharge under 1.5° and 2°C warming scenarios. All seasons, with the exception of summer, are expected to have increased discharge, with the largest increases occurring in spring. Regionally, Foxe Basin, under the 2°C scenario is expected to experience the largest increase in precipitation and river discharge.

In light of these current trends, it is still unclear as to the impact that these changes will have on the freshwater dynamics in this region. Although the contribution of river discharge is relatively small compared to sea ice melt on a seasonal time scale, the annual net freshwater flux is large. Thus, changes in river runoff, by seasonal and spatial redistribution, or long term trends, lead to changes in seawater density and stability. Saucier and Dionne (1998) studied the sensitivity of the region to a high runoff year and to regulated discharge, and found both to cause a decrease in salinity, along

with a general increase in sea ice thickness, both of which varied spatially and seasonally.

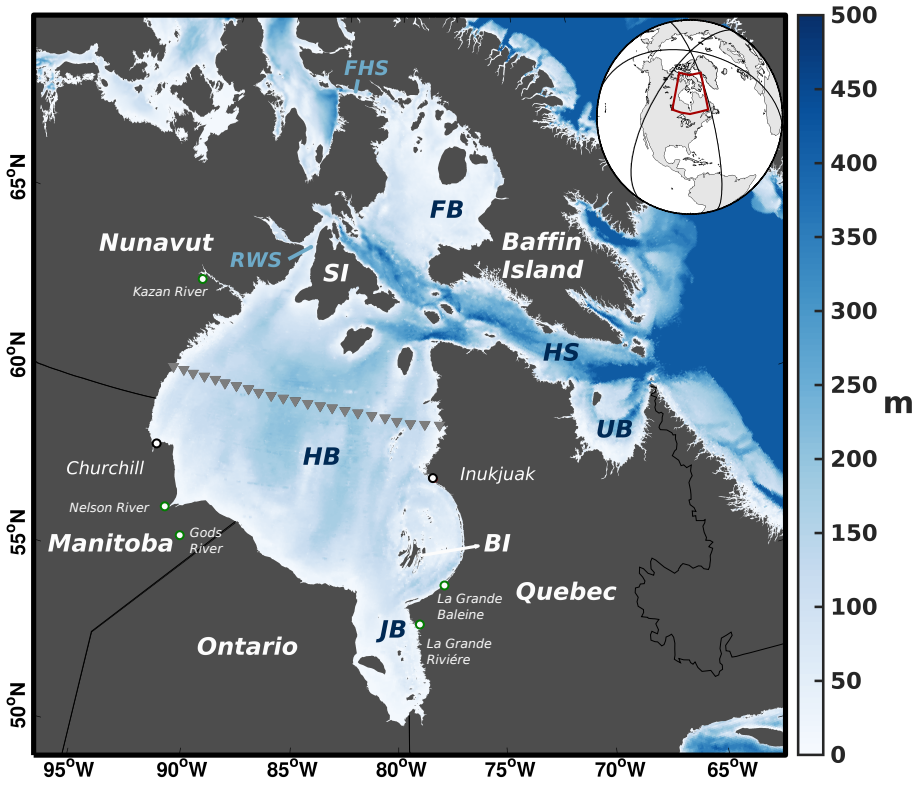

Figure 1: Bathymetry of the Hudson Bay Complex (HBC). FB denotes Foxe Basin, HS is Hudson Strait, UB for Ungava Bay, HB is Hudson Bay, and James Bay is shown by JB. Southampton Island is shown by SI. Fury and Hecla Strait is represented by FHS, and Roes Welcome Sound by RWS. Belcher Islands are denoted by BI. The towns of Inukjuak and Churchill are shown by the black rimmed circles, while river outlets are shown by green rimmed circles. Grey triangles show the model transect used for Figure 6.

To date, there have been no multi-year evaluations of the freshwater budget in this region. Other questions remain regarding the freshwater budget, for instance, how important are small scale processes in HBC dynamics?

Does the freshwater budget change with changes in river runoff? To have a better representation of the future of the region, we first need to know what is an appropriate model resolution in this region to capture the main processes, and what is the impact on the bay if there are spatial and temporal differences in river runoff entering the bay.

To determine the sensitivity of the HBC to runoff forcing as well as model resolution, we use a general circulation ocean model coupled with a sea ice model to evaluate the freshwater budgets, pathways, and boundary-interior exchange processes of each simulation. The following section contains a description of the model, as well as the various datasets used in the numerical experiments. In Section 3, an evaluation of the model and the freshwater budgets for each subregion in the HBC, as well as the main freshwater exchange processes in the Hudson Bay boundary and interior regions, are shown. Our analysis of the residence time is in Section 3.4, preceding the summary and conclusions. This work is part of the BaySys project, a bay-wide initiative to investigate effects of hydroelectric regulation and climate change on various aspects of the Hudson Bay environment, such as the biogeochemical, biological, and physical components of the system.

2. Method

2.1. Numerical Model

We use a general circulation ocean model, based on the Nucleus for European Modelling of the Ocean version 3.4 (NEMO; Madec and the NEMO team, 2008), which is coupled to the sea ice model, Louvain-la-neuve Ice Model version 2 (LIM2) with elastic-viscous-plastic (EVP) rheology (Hunke and

Dukowicz, 1997), and includes both thermodynamic and dynamic processes (Fichefet and Maqueda, 1997), for our simulations. The ocean model is hydrostatic and is a primitive equation model. We use the Arctic and Northern Hemisphere Atlantic (ANHA) configuration, which has two open boundaries, one at Bering Strait and the other at 20°S in the Atlantic Ocean. Two horizontal resolutions are used in our study, ¼° (ANHA4) and 1/12° (ANHA12) (Holdsworth and Myers, 2015; Dukhovskoy et al., 2016; Gillard et al., 2016; Müller et al., 2017; Hu et al., 2018), meaning the resolution within the HBC is 10–17 km for ANHA4 (Figure 2a), and 3.5–5.5 km for ANHA12 (Figure 2b). Vertically, there are 50 geopotential levels that have the highest resolution at the surface and decrease in resolution with increasing depth. For the vertical mixing scheme, we use a turbulent kinetic energy (TKE) turbulence closure scheme (Bougeault and Lacarrere, 1989; Gaspar et al., 1990; Blanke and Delecluse, 1993; Madec et al., 1998). Our simulations do not use temperature or salinity restoring so as to not damp the freshwater signals. Tides are also not included in these simulations as we will focus on large scale processes. We use 5-day averaged output from the model for our analysis, however, the time step for each resolution is 1080 seconds and 180 seconds for ANHA4 and ANHA12 respectively.

Our simulations are initialized with 2D (sea surface height and sea ice) and 3D (temperature, salinity, and horizontal velocities) fields from GLobal Ocean ReanalYsis and Simulations (GLORYS2v3) produced by Mercator Ocean (Masina et al., 2017). Boundary conditions, such as salinity, temperature, and ocean velocities are also provided by the GLORYS2v3 dataset. We use atmospheric forcing from the Canadian Meteorological Centre's (CMC)

global deterministic prediction system (GDPS) reforecasts (CGRF) described in Smith et al. (2014), along with CORE bulk formulae (Large and Yeager, 2004). This dataset provides 2 m air temperature and specific humidity, 10 m wind, downwelling shortwave and longwave radiation flux, and total precipitation to the surface at high temporal (hourly) and spatial (33 km) resolution. We integrate our simulations from January 2002 to December 2016. Monthly interannual runoff (described more in Section 2.2), as well as Greenland melt water provided by Bamber et al. (2012) is also carefully remapped onto the model grid to have more realistic freshwater input from land to ocean. The temperature of discharge when entering the ocean is given the same temperature as the surrounding sea water, typical of ocean general circulation models. Future improvements to the model will include the effect of discharge temperature to the ocean.

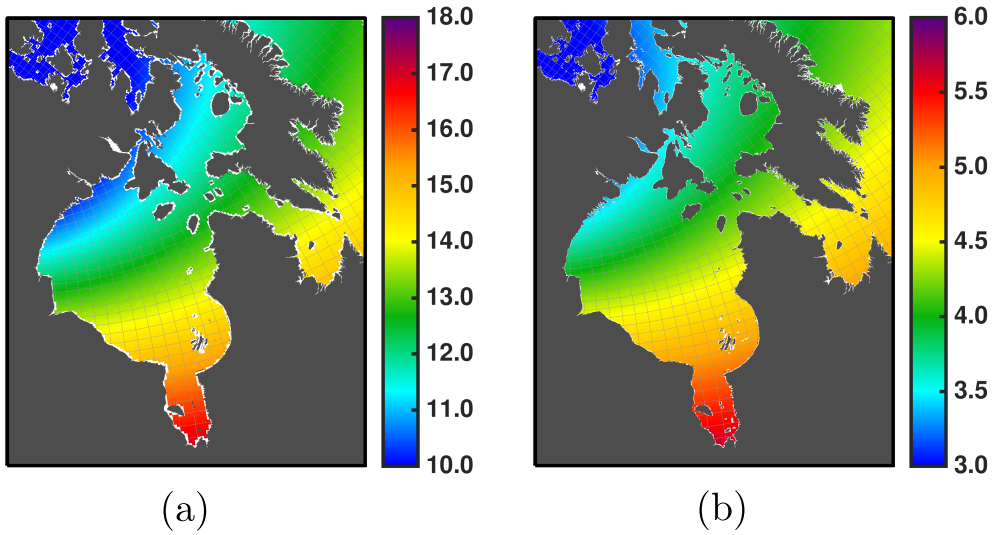

Figure 2: (a) ANHA4 and (b) ANHA12 configuration mesh for the HBC (every 5^{th} and 15^{th} mesh grid respectively), with colours showing model horizontal resolution in kilometers.

2.2. Runoff Datasets

To test the model sensitivity of the HBC freshwater budget to runoff forcing, we use three river discharge datasets: corrected Dai and Trenberth (referred to as DT; Dai and Trenberth, 2002; Dai et al., 2009), and two products from HYdrological Predictions for the Environment (HYPE; Lindström et al., 2010; Gelfan et al., 2017; Andersson et al., 2013) provided by BaySys Team 2. In this case, the HYPE model simulates stream flow for 398 streams and rivers draining into the HBC. One of the HYPE datasets used here is uncalibrated HYPE simulated stream flow that has been integrated with observed stream flow. Where observations are available, HYPE discharge is replaced with gap-filled observations from Déry et al. (2016). Gap-filled observations account for 45% of the mean annual discharge (58% of the HBC drainage basin) in this dataset. There are no discharge observations in Foxe Basin. We also note that observed discharge for La Grande Riviere (second largest river by volume) was not used. The uncalibrated HYPE model underestimates La Grande Riviere discharge and the engineered diversions are not fully represented in this version of the HYPE model. Thus, for the purposes of this study, this integrated, uncalibrated version of HYPE discharge will be referred to as HIUC. The second HYPE stream flow product used is from the calibrated version of HYPE, which we will refer to as HCAL. This runoff dataset has not been integrated with observations, but includes the improvements to the model, such as a better representation of La Grande Riviere discharge and Nelson River regulated discharge. HCAL discharge extends to 2013, while HIUC runoff extends to 2010. Thus 2010 runoff for HIUC, and 2013 runoff for HCAL, is used as forcing for the remaining years up to

2016. Similarly, as DT runoff only extends to 2007, runoff used in 2008–2016 is 2007 runoff. For consistency, throughout the study we compare the two HYPE datasets to DT, as DT is the standard river discharge dataset used for forcing ocean models. DT interannual runoff is used for the entire configuration for the control (CTRL) and high resolution (HIRES) experiments. The HYPE datasets are used in the HBC, with DT runoff used elsewhere in the third and fourth experiments (HIUC and HCAL). All four experiments use the Greenland melt water dataset described in Bamber et al. (2012). All runoff datasets are prescribed as monthly averages. A summary of the model experiments used in this study is shown in Table 1.

The seasonal cycles of the three runoff datasets used in the HBC in this study are shown in Figure 3. The DT discharge is larger than the HIUC discharge in most months, due to the gap filling strategy used for the dataset, most notably during the spring freshet, with differences peaking at 1.53 km^3/day in May. The difference between DT and HCAL also peaks in May at 1.07 km^3/day. All datasets show a secondary runoff peak in the fall, with the DT dataset having a more level peak spanning September and October. Throughout the year, DT discharge averages at 2.99 km^3/day (dark blue dashed line, Figure 3), HIUC averages at 2.45 km^3/day (light blue dashed line), HCAL has an annual average discharge of 2.54 km^3/day (green dashed line, Figure 3). This difference leads to nearly 200 km^3/yr more runoff in the DT dataset compared to HIUC, and over 150 km^3/yr compared to HCAL.

2.3. Residence Time Estimation

To estimate the residence time of river runoff in the HBC, we use an offline Lagrangian tool called Ariane (Blanke and Raynaud, 1997; Blanke et al.,

Table 1: Summary of model experiments. Time period used for analysis is 2004 to 2016. DT stands for Dai and Trenberth interannual runoff dataset.

Experiment	**Resolution**	**River Runoff**	**Atmospheric forcing**
HIUC	¼°	Integrated, uncalibrated HYPE in HBC, DT elsewhere	CGRF
HCAL	¼°	Calibrated HYPE in HBC, DT elsewhere	CGRF
CTRL	¼°	DT in the whole ANHA domain	CGRF
HIRES	1/12°	DT in the whole ANHA domain	CGRF

1999) to track water parcels from major river mouths. Even though Ariane only uses advection scheme tracking, with diffusion and mixing processes partly handled by the source (numerical model) velocity fields, it has been successful in tracing pathways of given water masses (Lique et al., 2010; Hu and Myers, 2013; Gillard et al., 2016; de Boisséson et al., 2012).

In this study, Ariane particles were released in January 2004, and tracked every 5 days based on 5-day averaged 3D velocity fields from CTRL until December 2016. Particles were released along the coastline where runoff forcing is applied. To avoid particles being trapped by the coastal cells, particles released in runoff forcing grid cells next to land cells were moved one cell away from the coast. Our results are based on releasing 50 particles per runoff grid cell in the top 10 m of the water column, so as to mimic

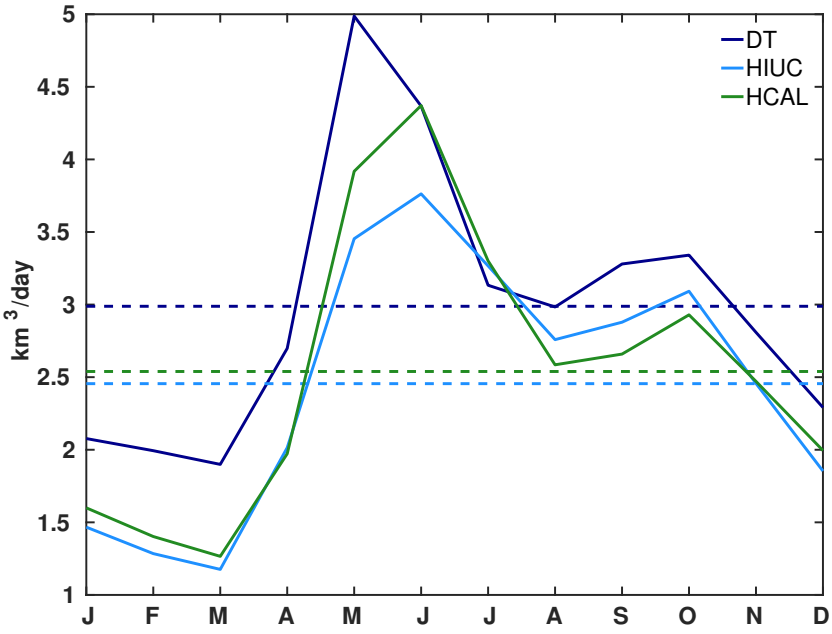

Figure 3: Seasonal cycle of the three runoff datasets used, averaged from 2004–2007, the common period of all datasets used, for the HBC. Dai and Trenberth discharge is represented by dark blue lines, where the solid line is the seasonal cycle and the dashed line is the mean discharge. Similarly, seasonal and mean HIUC discharge is shown by the solid and dashed light blue lines respectively, and HCAL by the green solid and dashed lines.

how runoff is dealt with in the model. Therefore, rivers with more discharge have more runoff grid cells and thus more Lagrangian floats assigned to the discharge.

2.4. Ocean hydrological observations

To evaluate the model simulations, we used observations comprised of ArcticNet cruise data (2005, 2006, 2007, and 2010 cruises; `http://www.arcticnet.ulaval.ca/`), Marine Environmental Data Service (MEDS, now Oceanography and Scientific Data or OSD; `http://www.meds-sdmm.dfo-mpo.`

gc.ca/) data from 1929–2015, and ICES Dataset on Ocean Hydrography (International Council for the Exploration of the Sea. Accessed March 14, 2016. Copenhagen, 2014. http://www.ices.dk) data from 1929–2016. Duplicate data in the dataset collection were removed.

Our evaluation of the ocean model includes comparing to available observations of temperature, salinity, and ocean velocities. Sea surface temperature (SST) data is satellite data from the Optimum Interpolation SST (OISST) Version 2 dataset (Reynolds et al., 2007) which are available from the National Oceanic and Atmospheric Administration (NOAA) Earth System Research Laboratory Physical Science Division (ESRL/PSD). The spatial resolution of this dataset is 0.25° and are based on the combination of the Advanced Very High Resolution Radiometer (AVHRR) infrared satellite and SST observations from ships and buoys. For salinity evaluation, observations between 1929–2015 from MEDS, were combined with data from ICES and ArcticNet Cruises, with locations shown in Figure 4. These data were then interpolated onto the ANHA grid in the HBC, for easier comparison with model simulations.

Ocean velocities were evaluated against altimeter products, absolute geostrophic velocity, produced by Ssalto/Duacs and distributed by Aviso with support from Cnes (http://www.aviso.altimetry.fr/duacs/). These data were daily with a ¼° spatial resolution.

2.5. Ice Observations

We evaluated simulated sea ice drift through comparison with the low-resolution sea ice drift product of the EUMETSAT Ocean and Sea Ice Satellite Application Facility (OSI-SAF, www.osi-saf.org). With a spatial reso-

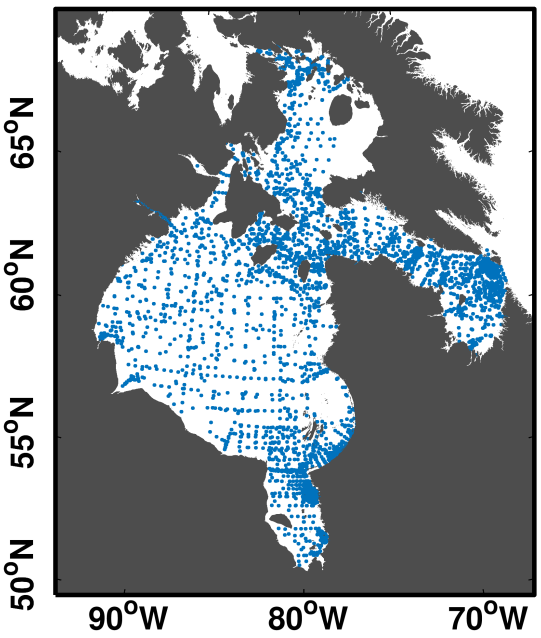

Figure 4: Locations of salinity point measurements used for Figure 5.

lution of 62.5 km, and time lapse of two days, the OSI-SAF sea ice drift product combines data from daily maps of satellite signals, including brightness temperatures from passive microwave sensors, or radar backscatter from scatterometers (Lavergne et al., 2015). A continuous maximum cross correlation approach is implemented to provide continuous spatial coverage between subsequent satellite sub-images. Accuracy and validation of the ice drift product are determined from comparison with ice beacon trajectories and observations. Uncertainty maps are provided with the OSI-SAF sea ice drift product. Uncertainty in zonal and meridional displacements is on the order of 2.5 km.

Sea ice thickness observations were obtained for the period November

2010–April 2016 from a combination of Cryosat-2 Synthetic Aperture Interferometric Radar Altimeter (SIRAL) Baseline C data and Soil Moisture and Ocean Salinity (SMOS) L-band radiometer data. The full processing chain for deriving and merging these thickness products for the HBC region is provided in Landy et al. (2017). Briefly, sea ice and ocean (lead) returns from SIRAL are classified according to the shape of the radar echoes, before ice/water surface height above a reference Earth ellipsoid is 'retracked' from the echo leading edge. Various corrections are applied to the elevation observations for known geodetic and oceanographic biases, including geoid undulations, tides, dynamic topography of the ocean and the inverted barometer effects. Sea ice freeboard is obtained by subtracting the sea level (from lead tie-points) from the sea ice surface elevation, and is finally converted to ice thickness using assumptions for sea ice, snow and ocean densities, and DMSP/SSMIS observations of snow depth. Thin sea ice thickness can be derived from SMOS from a theoretical relationship between L-band brightness temperature and ice thickness, including a number of assumptions concerning the ice thermodynamics and concentration. Ice thickness data up to a maximum thickness of 1 m was obtained from the Integrated Climate Centre at the University of Hamburg (Tian-Kunze et al., 2013). Ice thickness from the two datasets were merged between November and January (i.e. when thin ice is prevalent in the HBC), only where Cryosat-2 ice thickness was $<$ 1 m.

Simulated ice concentrations were compared to ASI Algorithm AMSR-E/AMSR2 sea ice concentration, which were obtained for 2002–2015 from the Institute of Environmental Physics (`https://seaice.uni-bremen.de/`

sea-ice-concentration/), University of Bremen, Bremen, Germany (Spreen et al., 2008). AMSR-E data is used from January 2004 to October 2011, and AMSR2 data is used from July 2012 to December 2015. AMSR-E/AMSR2 ice concentration data has a horizontal resolution of 6.25 km and a temporal resolution of 1 day.

2.6. Reference Salinity

We use a reference salinity of 33 for our freshwater calculations as this is the most saline layer in Hudson Bay and has been used by earlier studies (St-Laurent et al., 2011; Granskog et al., 2007; Prinsenberg, 1984). The freshwater fluxes are the product of the area of the side of the grid cell, the perpendicular velocity, and the grid cell's freshwater concentration, defined as

$$FW = \frac{S_{ref} - S}{S_{ref}} \tag{1}$$

where FW is the freshwater concentration. The reference salinity is represented by S_{ref} which we use 33, and the seawater salinity as S.

3. Results

3.1. Model evaluation

To evaluate the model, we first show spatial sea surface temperature (SST) for the model and observations in Figure 5a-j for both summer and fall. During the winter (January, February, March) and spring (April, May, June), the simulated SSTs are at the freezing point (not shown) since the bay is ice covered. In fall, simulated SSTs (Figure 5a-d) agree very well with observations (Figure 5e). The temperature gradient from north to south in

Hudson Bay is captured well by all simulations. Most simulations are too cold along the northern coast of Hudson Strait, as well as simulate colder SSTs along the western coast of Foxe Basin compared to observations.

In summer, the general pattern of the simulated SST tends to follow the observed SST pattern, i.e. showing higher temperatures in James Bay and lower temperatures in northern Hudson Bay, Hudson Strait, and Foxe Basin (Figure 5f-j). There are some inconsistencies as well. On the large scale, simulations show colder SSTs compared to observations, such as in central Hudson Bay where SSTs are approximately 3°C colder than observations in all simulations, due to the heat flux associated with CGRF atmospheric forcing. Moreover, the coastal areas in northwestern and southwestern Hudson Bay, and in southern James Bay and Ungava Bay, show higher temperatures in all simulations compared to observations. Along the eastern shore of Hudson Bay, all simulations are colder than observations, with the exception of northeast of the Belcher Islands.

Figure 5k-o shows the spatial distribution of the top 100 m averaged salinity for observations and four experiments. Observations from July to September are shown, while only August is shown for model experiments. This was done because the majority of observations were taken in August (450,000 measurements from all depths), but a significant number of observations were taken in July and September (25,000 and 200,000 measurements respectively), which were included for more spatial coverage.

The bottom panels in Figure 5 show top 100 m salinity in the summer. All four model experiments capture the higher salinities in the center of Hudson Bay, western Foxe Basin, and the northern coast of Hudson Strait. The

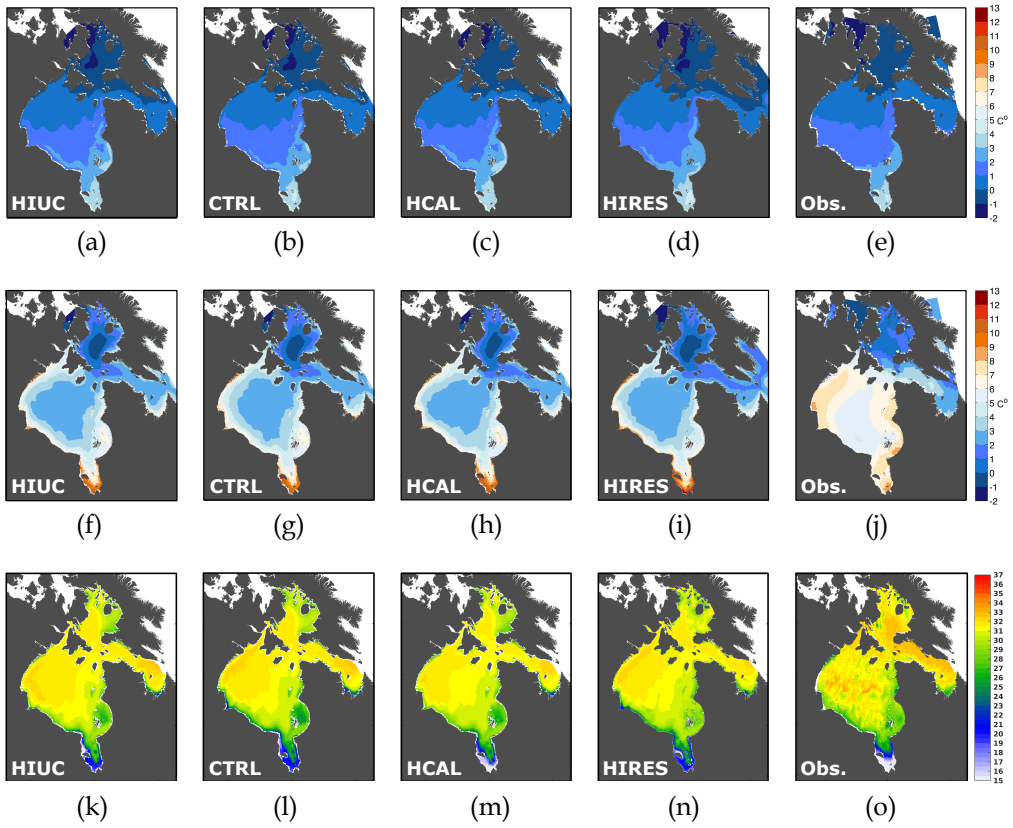

Figure 5: Fall (October, November, December) SST for four model experiments (a) HIUC, (b) CTRL, (c) HCAL, (d) HIRES, and (e) observations. Summer (July, August, September) SST for four model experiments (f) HIUC, (g) CTRL, (h) HCAL, (i) HIRES, and with observations shown in (j). The bottom panel shows top 100 m mean salinity for August 2004–2016 for model experiments (k) HIUC, (l) CTRL, (m) HCAL, and (n) HIRES, and in (o) available gridded July–September observations.

experiments also simulate the low salinities observed along the southern coast of Hudson Bay, and in James Bay. Smaller features, such as low salinities east of the Belcher Islands, north of Inukjuak, eastern Foxe Basin, and southern Ungava Bay are also captured by the experiments.

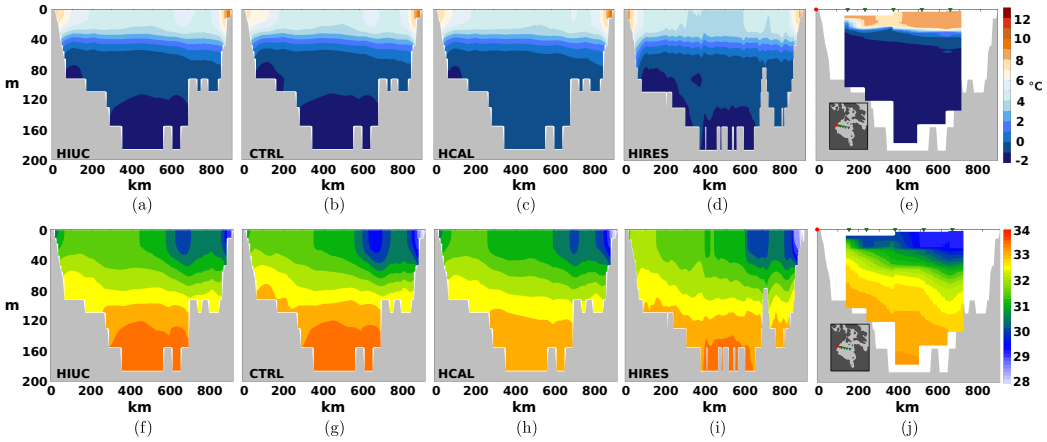

Figure 6: Mean temperature and salinity cross sections for the (a,f) HIUC, (b,g) CTRL, (c,h) HCAL, and (d,i) HIRES simulations for September 8–12, 2006. Observations (e,j) shown are from a transect spanning from September 8–10, 2006. The x–axis shows the distance in kilometers from the red circle shown in (d,i), and observed profiles were taken at the points marked with green triangles in the inset.

Data from an ArcticNet Cruise in September 2006 (`http://www.arcticnet.ulaval.ca/`) were used to compare a west–east cross section in Hudson Bay with the model simulations (Figure 6). Observations show warmer surface temperatures and cooler temperatures at depth (Figure 6e) compared to all model simulations (Figure 6a-d). This could be due to an issue with the air-sea fluxes or that the model uses 5 day averages, instead of single point measurements at a given time. Another possible explanation for this discrepancy is that the model overestimates vertical mixing. All model simulations show warmer surface temperatures along the coast, which is not available in the observations. The depth of the mixed layer in model simulations, around 40 m, is close to the observed mixed layer depth seen in Figure 6e. The transition between the warm surface waters and the cooler waters at depth

is more abrupt in observations compared to the model simulations as well.

Figure 6f-i shows salinity along the same west–east cross section in Hudson Bay for the HIUC, CTRL, HCAL, and HIRES simulations. Bathymetry is different in the HIRES simulation due to the higher resolution. Three of the four simulations show salinities higher than 33.5 at the bottom, while the HCAL experiment and observed salinities do not exceed this value. In this 5-day mean snap shot, salinities at the surface are also higher than observations, with closer agreement towards the east coast. The model captures the isohaline slopes at intermediate depths very well, which are generally at comparable depths to observations.

AVISO geostrophic currents in Figure 7 (red) are compared to simulated geostrophic velocities shown in yellow. All simulations show weaker geostrophic velocities in central Hudson Bay compared to the AVISO geostrophic velocities. In all cases, flow along the southern coast of Hudson Strait is stronger in the model than observations, as well as along the western Hudson Bay coast.

The root mean square error (RMSE) for zonal and meridional velocities is shown in Table 2. For all simulations, the RMSE is larger in the meridional direction compared to the zonal direction. RMSE values are comparable between the ¼° experiments, while HIRES has the largest values in both the meridional and zonal directions.

The HBC ice concentration seasonal cycle is shown in Figure 8a. Simulated ice concentration is less than observed in the first three months of the year, for all experiments. The HIRES experiment has the best agreement with observations for January–May. During the melt season, ice concen-

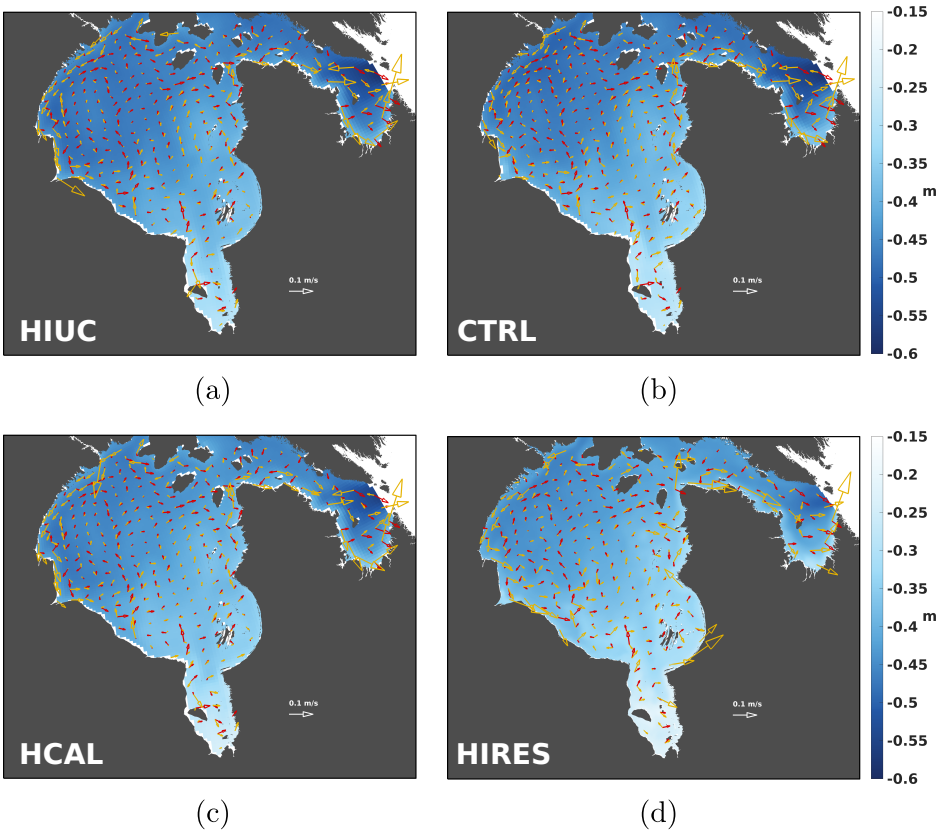

Figure 7: Simulated July-September mean surface geostrophic velocities (yellow) and sea surface height with AVISO vectors in red for (a) HIUC, (b) CTRL, (c) HCAL, and (d) HIRES. Velocities, both observed and simulated, were averaged over 2004–2015.

trations are up to 5% lower than observations, while during the ice growth season in the fall, simulated ice concentrations are significantly lower, particularly in December with an ice concentration difference of over 30%. This discrepancy can be explained by the late ice formation in the fall in our model configuration. This late ice formation is also seen in the seasonal cycle of ice thickness (Figure 8b), where we have differences of over 20 cm in December, with all simulations underestimating ice thickness to the same degree.

Table 2: Root Mean Square Error (RMSE) between July-September (2004-2015) mean simulated surface geostrophic velocities and AVISO geostrophic velocities (regions below 64°N). Units are in cm/s.

Experiment	**Zonal $\pm$ 1σ**	**Meridional $\pm$ 1σ**
HIUC	4.8 $\pm$ 9.3	7.0 $\pm$ 18.8
CTRL	4.8 $\pm$ 9.1	7.0 $\pm$ 18.8
HCAL	4.8 $\pm$ 9.1	6.9 $\pm$ 18.7
HIRES	5.0 $\pm$ 9.5	7.6 $\pm$ 20.0

Underestimations of ice thickness continue to occur throughout the winter, however the difference between observations and the model simulations decreases in March and April. The two simulations using the DT runoff have marginally thicker ice in March compared to the two simulations that use the HYPE discharge datasets.

We focus on the model skill in capturing the sea ice growth and melt periods. As the HBC is ice free in summer, and ice covered in winter, it is the transition times that are crucial for biology, such as algal and phytoplankton blooms, krill, fish, and polar bears, as well as industry, such as shipping. Figure 9 (top panels) shows the mean ice concentration for April–June. Observations Figure (9e) show high ice concentrations in Foxe Basin during this time, which all model simulations capture. Observations show lower ice concentrations on the northern coast of Hudson Strait, and higher concentrations along the southern coast, of up to 70%. All model simulations show too much ice in Hudson Strait, and the north-south structure is not completely captured. During this time, high concentrations of ice are still observed in central Hudson Bay, of up to 95%, which the model runs

are able to simulate. Finally, observations show James Bay with low ice concentrations along the southern and eastern coasts, and higher concentrations in the northwest corner. The simulations overestimate ice concentrations in James Bay during this time of year.

Ice concentrations during the ice growth season, from October–December, are shown in Figure 9f-j. As has been stated previously, the late ice formation in our model simulations is a known issue. Ice concentrations in Foxe Basin are well simulated in all model experiments. Hudson Strait has ice concentrations that are higher than observations, especially near its eastern gate, but overall model simulations are comparable to observations in this region. Larger differences between the model and observations occur in Hudson Bay. Higher ice concentrations, between 40-50%, in northwestern Hudson Bay are not captured, as well as the higher concentrations across the bay, which is due to late freeze up in the model. However, the progression of ice concentrations across the bay from east to west is captured by the model simulations.

Spatial ice thickness is shown in Figure 9k-o for the months January–April. The model is able to reproduce thinner ice in western Hudson Bay where there is a recurrent polynya. All experiments show thicker ice in eastern relative to western Hudson Bay, specifically east of the Belcher Islands. The observations show thicker ice from the center of the bay to the eastern coast, of which all experiments are not able to simulate. Additionally, thicker ice in the interior, between 1.5–2 m is not captured as simulated ice thickness ranges from 0.8–1.2 m. Thicker ice along the eastern coast of Ungava Bay is captured by all experiments, with approximately the same magnitude. Ice thickness in Hudson Strait is simulated well, with the exception of the north-

western portion, where observations show ice thickness exceeding 2.5 m. In Foxe Basin, thick ice is located in the eastern region in observations, the location of which was captured in the model experiments. However, simulated ice thickness is up to 1 m thinner compared to observations.

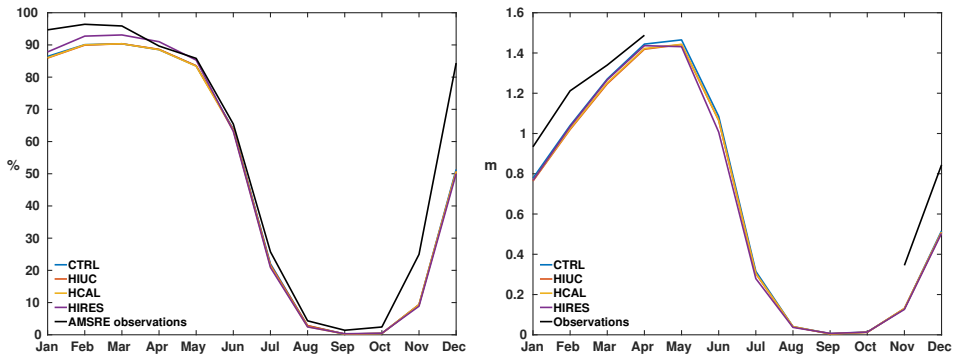

Figure 8: Seasonal cycle of (a) ice concentration and (b) thickness in the HBC for model experiments and observations (black). HBC ice concentration for simulations and AMSR-E/AMSR2 observations is averaged over 2004–2015, while for ice thickness, simulations and observations were averaged over 2011-2015.

Next we show the ice thickness distributions (ITDs) in Hudson Bay for January–April (Figure 10a-d), with observations shown in grey. All model simulations are unable to simulate the width of the ITD in observations, to compensate for this, the peak fraction of the ice thickness is higher than observations. We will note that the simulated peak ice thickness is close to the peak ice thickness in the observations. The HIUC simulation shows lower fractions of thicker ice from January to April, compared to the other experiments, however the fractions of the peak ice thickness are larger. The CTRL experiment has higher fractions of ice thickness around the mode

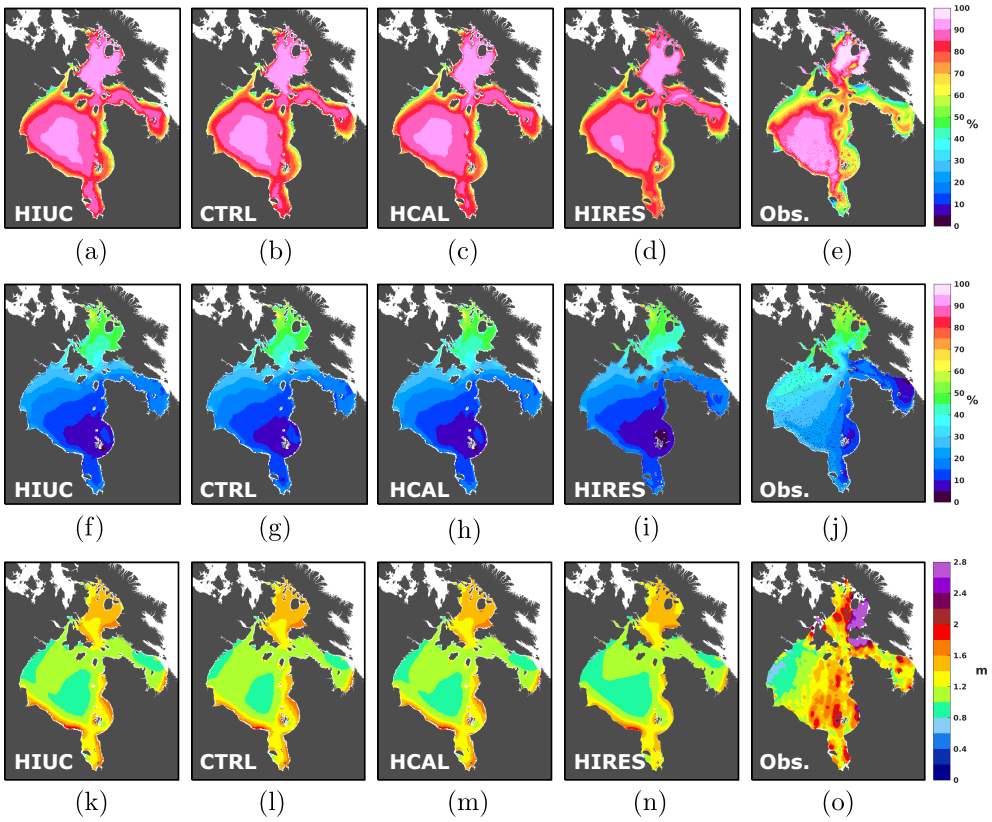

Figure 9: Top panels (a-e) show mean April–June ice concentration averaged from 2004–2011 HIUC, CTRL, HCAL, HIRES, and AMSR-E/AMSR2 observations. Center panels (f-j) shows the October–December ice concentration counter part to the top panels. In the bottom panels (k-o), mean January–April ice thickness (2011-2015) for HIUC, CTRL, HCAL, HIRES, and observations.

compared to HIRES, indicating the role of small scale processes in producing thinner ice.

The amount of freshwater stored in ice is important for the seasonal freshwater budget, and thus, should be simulated correctly. Landy et al. (2017) used sea ice thickness observations to calculate the amount of freshwater

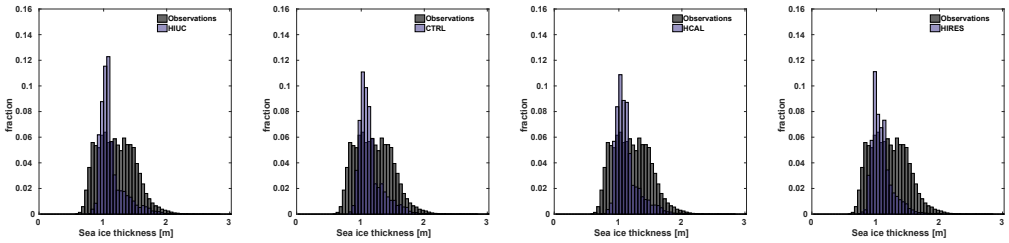

Figure 10: January–April (2011–2015) ice thickness distribution in Hudson Bay for (a) HIUC, (b) CTRL, (c) HCAL, and (d) HIRES shown in purple and observations shown in grey.

stored in HBC sea ice in April, the time of maximum sea ice volume, before melt onset. They found the volume of freshwater to be 1253 ± 15 km^3 for the end of April. Following their calculation

$$V_{lfw} = V_i\Big(1 - \frac{S_i}{S_{ref}}\Big)\frac{\rho_i}{\rho_{sw}} \tag{2}$$

where V_{lfw} is the volume of liquid freshwater and V_i is the volume of ice. In our model, S_i is fixed at 6, and we used S_{ref} as 33, as Landy et al. (2017) did. Finally, model ice density is 900 kg/m^3, and given by ρ_i, while seawater density is given as ρ_{sw}, where we use 1024 kg/m^3, following Landy et al. (2017). For our calculation we use the mean ice volume for April 2004-2015, and the results are shown in Table 3. Our results agree very well with their observational estimate, with all simulations within 70 km^3 of the observational estimate. CTRL contains the most freshwater in sea ice in April, while HIRES contains the least, which agrees best with observations, indicating the importance of resolution. Volume of runoff, as well as the timing and location of its release in the bay impacts the volume of freshwater in ice, as both HCAL and HIUC have less runoff than CTRL and thus have

Table 3: Liquid freshwater equivalent (± 1 standard deviation) contained in HBC sea ice in April (2004–2015) in units of km^3.

Experiment	$\mathbf{V}_{fw} \pm \mathbf{1}\sigma$
HIUC	1306 ± 112
CTRL	1323 ± 112
HCAL	1300 ± 107
HIRES	1285 ± 115
Landy et al. 2017	1253 ± 15

a lower volume of freshwater in ice. However, the HCAL simulation receives more discharge than HIUC, yet HIUC contains more freshwater in the ice.

We compare simulated ice drift to the OSISAF observational dataset (Figure 11). General sea ice circulation features are captured by all model simulations, with regional differences in ice drift patterns (Figure 11). An evaluation of root mean square error (RMSE) and bias (not shown) shows northwest/southeast asymmetry in drift and error distribution, comparable to Saucier et al. (2004), as well as sensitivity to model resolution, with local differences in response to runoff forcing.

Evaluation of zonal and meridional RMSE maps show that uncertainty in ice drift is governed by meridional drift in northwestern (low) and central (higher) Hudson Bay, and by zonal drift in southeastern (maximum) Hudson Bay. Higher meridional RMSE values are observed in central and eastern Hudson Bay for the HIRES experiment, and in southwest Hudson Bay for the HIUC experiment. The authors speculate that maximum RMSE values in the zonal ice drift component in northwestern Hudson Bay may be attributed

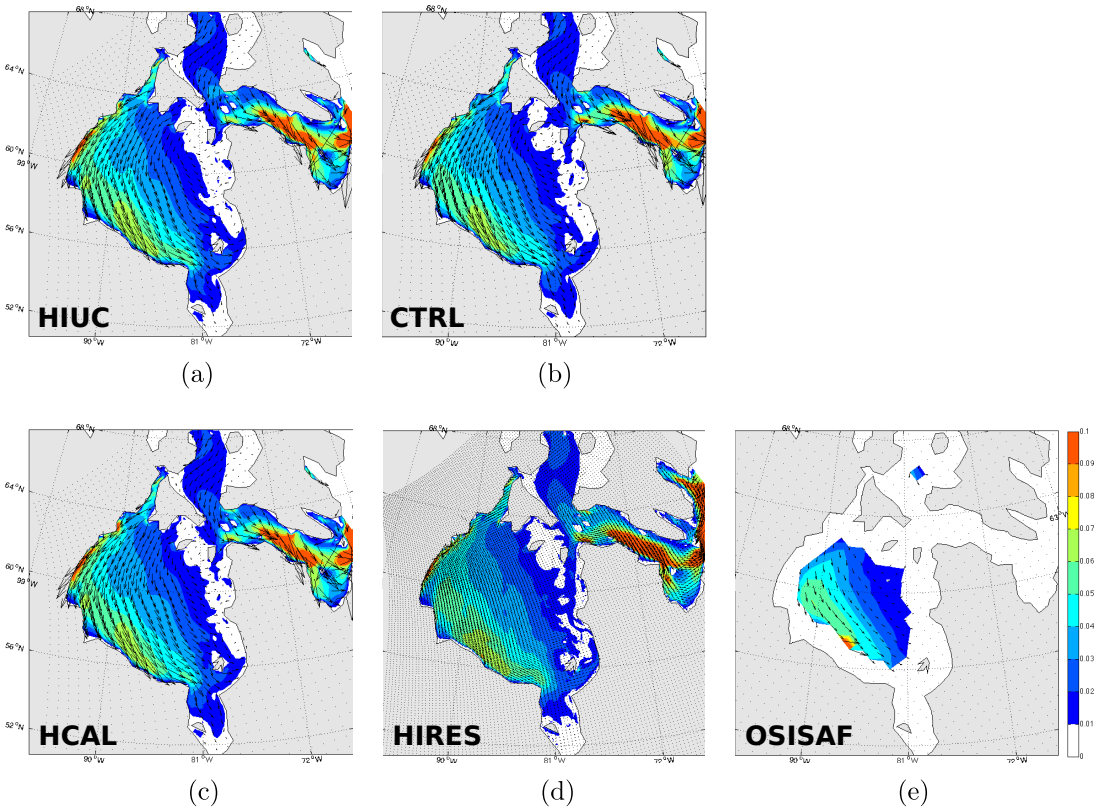

Figure 11: Mean 2007-2015 January-March ice drift vectors (arrows) and speed (colours) for (a) HIUC, (b) CTRL, (c) HCAL, (d) HIRES, and (e) OSISAF observations in units of m/s.

to deformation processes associated with delayed ice formation in fall and subsequent interactions between landfast and pack ice in winter. Enhanced RMSE in the zonal ice drift component in southeast Hudson Bay may be attributed to representation of sea ice dynamics and deformation in particular in the LIM2 sea ice model.

Based on the above model evaluation, we acknowledge the larger discrepancies between observations in sea ice in fall, however, we find over all, with

the volume of equivalent freshwater in sea ice in April as well as spatial ice concentration and thickness in the bay, that the model is able to capture and simulate the main features in the ice cover. Similarly, oceanographic variables, such as temperature, salinity, and velocities, are also simulated well. Thus we find that based on our evaluation, this model is able to correctly simulate the main dynamics and features in the bay so as to be used to investigate the freshwater budget in this region.

3.2. HBC annual freshwater budget

The freshwater budget for the HBC and its subregions takes the form

$$\text{advected freshwater} + \text{surface flux} + \text{runoff} - \text{FW storage} = 0 \quad (3)$$

where runoff is a freshwater source, while advected freshwater, which depends on both salinity and the direction of flow, and surface fluxes (precipitation minus evaporation and sea ice growth/melt) can be sources or sinks. The right hand side is the storage of freshwater in the basin. This last term is not a flux, but just the amount of freshwater that is stored in the basin. For the purposes of this paper, negative fluxes are defined as leaving the region, and positive fluxes as entering the region, unless otherwise specified.

3.2.1. Impact of runoff on surface and lateral fluxes

Annual freshwater budgets for the HBC and its subregions were calculated for the three ¼° experiments, and are shown in Figure 12. The HBC, as a whole, receives about 22% (200 km^3/yr) more runoff in CTRL compared to the HIUC experiment. The HIUC runoff dataset has less runoff entering the HBC in all months, especially during peak runoff in spring and early fall

(Figure 13a). The one exception is Hudson Strait, where the HIUC runoff is larger than the DT dataset by 8% (20 km^3/yr). The HCAL experiment has about 3% (20 km^3/yr) more runoff entering the HBC as a whole compared to HIUC. However, separating into subregions shows that CTRL has the least amount of runoff entering Hudson Strait, followed by HCAL and HIUC. In Hudson Bay, HCAL has 28% (110 km^3/yr) less runoff than CTRL. Foxe Basin, on the other hand, has the most discharge in the HCAL simulation, 35% (30 km^3/yr) and 56% (50 km^3/yr) more than the CTRL and HIUC experiments respectively. Lastly, the DT dataset has the most runoff in James Bay of 360 km^3/yr, compared to both HYPE products which have 213 and 224 km^3/yr for HIUC and HCAL accordingly.

Surface fluxes are larger in the HBC, as a whole, in the HIUC experiment, followed by HCAL. The separate basins show higher net surface fluxes in Hudson Bay (13 km^3/yr or 12%) and James Bay (5 km^3/yr or 7%) in the HIUC simulation compared to CTRL, with no change in Hudson Strait surface fluxes. Surface fluxes in Hudson Bay in HCAL are similar to HIUC, while HCAL surface fluxes in James Bay are comparable to CTRL. Of the ¼° simulations, HCAL has the lowest magnitude of surface fluxes, at -2 km^3/yr in Hudson Strait. Foxe Basin surface fluxes show little change between the CTRL and HIUC experiments, while HCAL has the largest net negative surface flux.

Advected freshwater out of the HBC, as a whole, is 18% (140 km^3/yr) larger in the CTRL experiment than HIUC. This is also the case for freshwater advection in both Hudson and James Bays, with 21% (82 km^3/yr) and 41% (147 km^3/yr) more river discharge per year respectively. Advected

freshwater in the HCAL simulation falls between CTRL and HIUC for Hudson Bay, and the HBC as a whole. Advection in James Bay for HCAL is 9% (25 km^3/yr) larger than HIUC, with CTRL having even more advected freshwater out of the shallow bay. On its own, Hudson Strait has more freshwater advection out of the strait in HIUC, by 18% (40 km^3/yr), than CTRL, due to less freshwater storage and more runoff, with HCAL falling in between. HCAL is only the simulation to have net advection out of Foxe Basin of the three ¼° experiments of -3 km^3/yr, with the CTRL experiment advecting 45% (13 km^3/yr) less into the basin than the HIUC experiment. The sum of the advected freshwater, surface fluxes, and runoff, equals the amount of freshwater that is stored in each region. CTRL has higher freshwater storage values overall than HIUC and HCAL, with the exception of Foxe Basin, where HCAL has the highest freshwater storage of the ¼° experiments.

Figure 13 shows the seasonality of each of the freshwater terms in the freshwater budget equation. In regions such as the HBC and Hudson Bay proper, surface fluxes are the dominant term throughout the year, with maxima in June and minima in December. In the HBC, advected freshwater and runoff are approximately in balance, with different runoff datasets having very little impact on the seasonality of advected freshwater (Figure 13a). As Foxe Basin is farther north, peak surface fluxes occur in July (Figure 13c) and are minimum in November, and like Hudson Bay proper, surface fluxes are the dominant term. The DT and HCAL datasets show a runoff peak in June in Foxe Basin, whereas, there is no clear peak in the HIUC runoff. This difference appears not to have a large impact on advected freshwater in the region, as peak net advection into the basin occurs in August in all

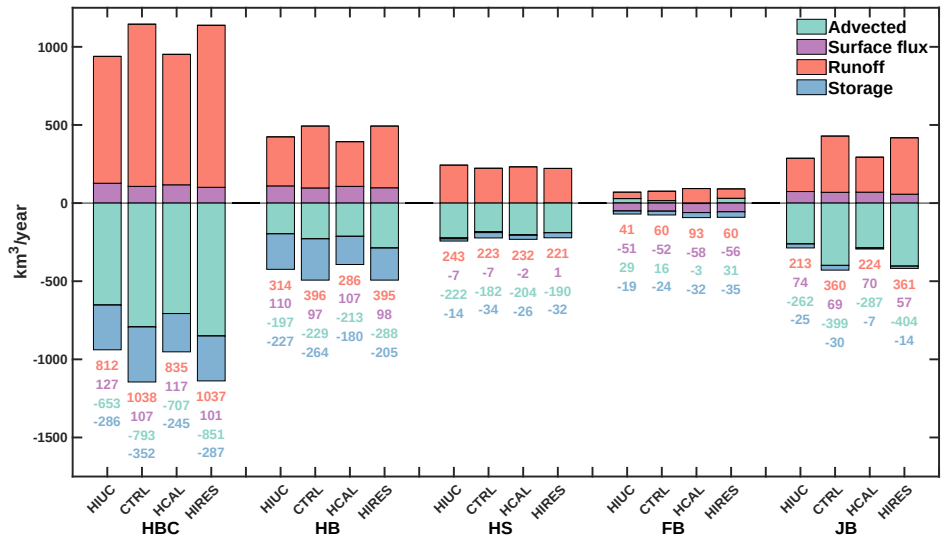

Figure 12: Annual freshwater budget for the HBC, Hudson Bay (HB), Hudson Strait and Ungava Bay (HS), Foxe Basin (FB), and James Bay (JB), for each of the four experiments. Units are km^3 per year, with a reference salinity of 33. Time period is 2004–2016.

simulations, with maximum freshwater export out of the basin occurring in November. Similar to the HBC seasonal cycle, Hudson Bay proper runoff and advected freshwater are roughly balanced during winter, with maximum freshwater export occurring in October and December for all experiments. However, during summer, freshwater export weakens and there is a net freshwater import into the bay. This occurs because of the large amount of freshwater that is advected out of James Bay (Figures 13e) and into Hudson Bay. During the year, surface fluxes in both James Bay and Hudson Strait are not as dominant in the freshwater budget as the other basins (Figure 13). Surface fluxes peak in June in both regions with minima in December and January for all experiments. Runoff seasonality in both basins is reduced in the HIUC experiment compared to CTRL, due to the more 'damped' seasonal

cycle in the runoff dataset, with HCAL having more seasonality than HIUC, but less than CTRL. Advected freshwater in Hudson Strait varies between simulations, with CTRL advecting more than the other two ¼° experiments, likely due to the gap filled DT dataset, and is more noticeable in the winter months. Similarly, advected freshwater in James Bay is also reduced in HIUC and HCAL compared to the CTRL simulation throughout the year, due to the impacts of regulation included in the HYPE datasets. The advection is directly related to the runoff, with peak advection occurring one month later than peak runoff in both summer and fall. Peak runoff in CTRL causes maximum freshwater storage in May, one month earlier than both the HIUC and HCAL experiments. In this study, our focus is on the long term mean, however, investigating year-to-year variability in the freshwater budget would be an interesting topic for future work.

Figure 14 shows the freshwater advection for each gate in the HBC for the four experiments (gates are indicated in Figure 13f). Freshwater and volume transport through Fury and Hecla Strait are similar for the HIUC, HCAL, and CTRL experiments, while freshwater transport through Southampton and Baffin Islands are similar between the HIUC and CTRL experiments. The HCAL experiment has 0.1 mSv more freshwater transport through this gate compared to the other two. Volume transport, on the other hand, varies, with CTRL having 7.4 mSv less volume transport than HIUC through Baffin–Southampton Gate, while HCAL has 1 mSv less transport compared to HIUC. Flow through Roes Welcome Sound is similar between HIUC and HCAL with regards to freshwater transport, but there is more volume transport, by 2.6 mSv, in HCAL. CTRL has a larger volume flux by 7.2 mSv com-

pared to HIUC, in addition to 0.5 mSv more freshwater transport through the sound. Freshwater and volume fluxes through the Southampton–Quebec gate, James Bay, and eastern Hudson Strait are all smaller in the HIUC experiment compared to CTRL, which is due to the HIUC dataset having less runoff, as this dataset does not include regulation on the La Grande Riviere. Fluxes through the three eastern gates in the HCAL experiment fall between HIUC and CTRL. A detailed comparison of fluxes obtained here and available observations is presented in Section 4.

3.2.2. Impact of model resolution on surface and lateral fluxes

The CTRL and HIRES experiments have the same runoff forcing, and thus the same volume of runoff entering each region every year (Figure 12). HIRES has more advected freshwater out of the HBC by roughly 7% (60 km^3/yr). The difference leads to less, by roughly the same amount, freshwater storage in the HBC in the HIRES experiment, compared to CTRL. In the subregions, runoff and surface fluxes are similar in Foxe Basin, while advected freshwater is about twice as much as in CTRL. Freshwater storage is also larger in HIRES compared to CTRL by 31% (11 km^3/yr) in Foxe Basin. In Hudson Strait, runoff is similar while advected freshwater is 4% (8 km^3/yr) higher than CTRL. Surface fluxes are close to zero in HIRES, and are a freshwater source, whereas CTRL surface fluxes are a freshwater sink and have a magnitude of 7 km^3/yr. Freshwater storage in the strait is similar between the two runs, at 34 km^3/yr in CTRL and 32 km^3/yr in HIRES. Both surface fluxes and runoff are the same in Hudson Bay. Advected freshwater, however, is larger in the HIRES simulation compared to CTRL by 20% (60 km^3/yr), leading to less freshwater storage in the HIRES simulation.

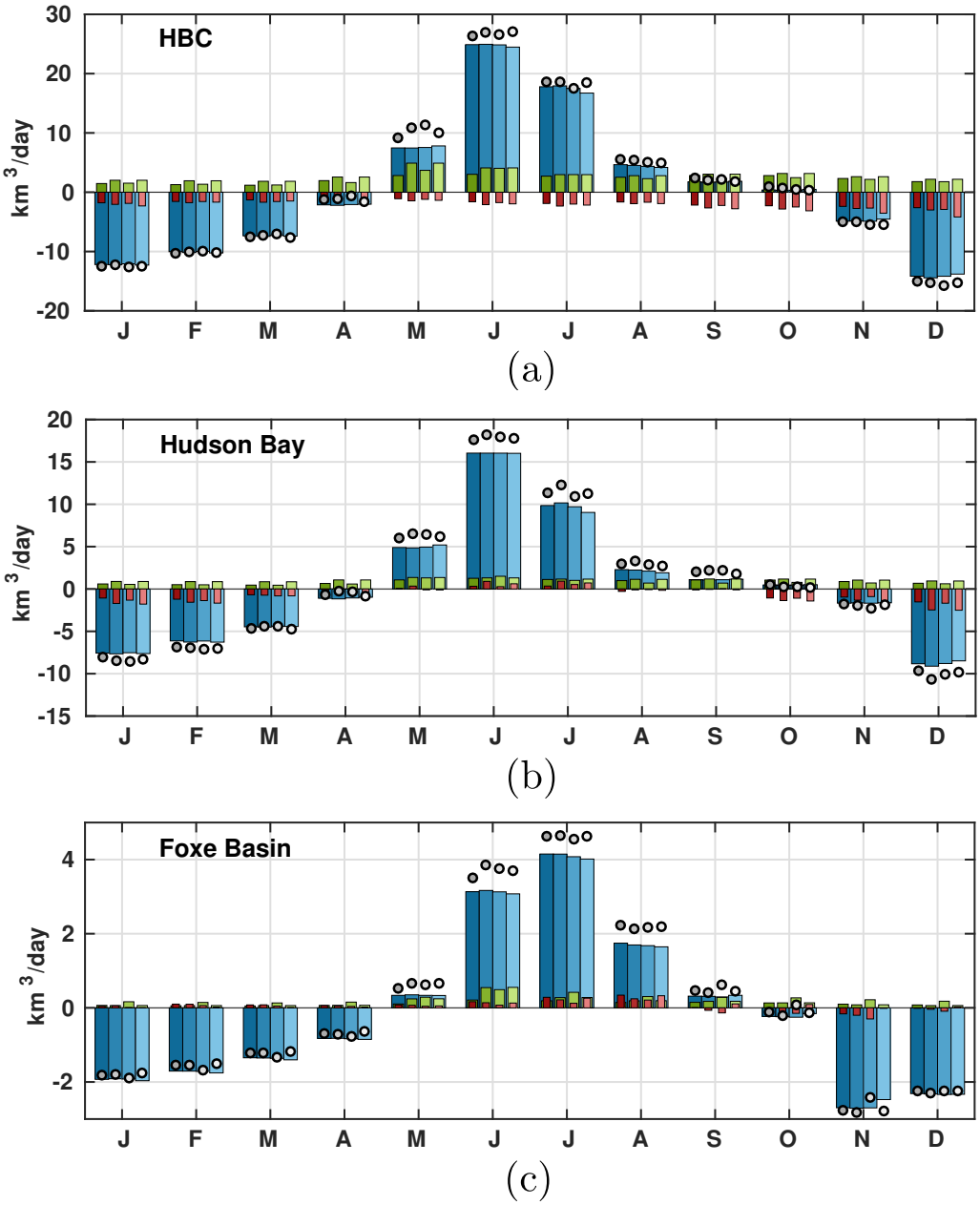

Figure 13: Seasonality of the freshwater budget terms (2004–2016) for four experiments in each region, (a) HBC, (b) Hudson Bay, (c) Foxe Basin, (d) Hudson Strait, and (e) James Bay (e). A map showing the definition of each region is shown in (f) with various gates indicated. Each term in the freshwater budget is is shown by a different colour, with blue bars showing surface fluxes, river runoff as green bars, red bars as advected freshwater, and grey circles showing the freshwater storage in each basin. Experiments are ordered as HIUC, CTRL, HCAL, and HIRES (darkest to lightest shade) from left to right in each set of bars.

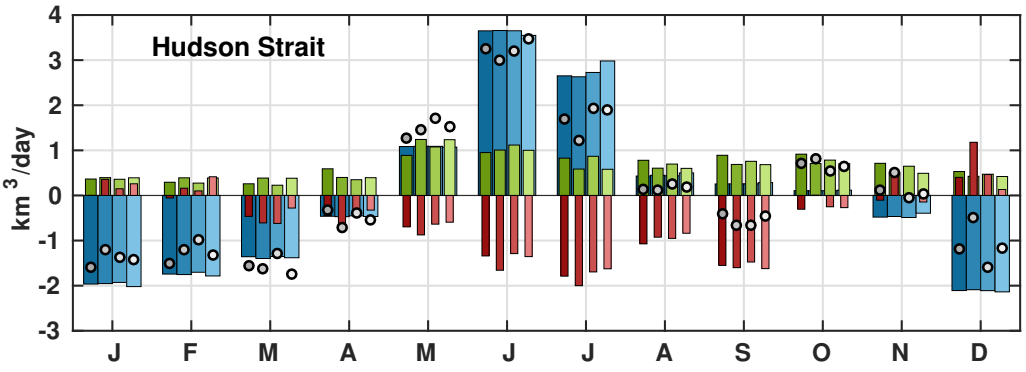

(d)

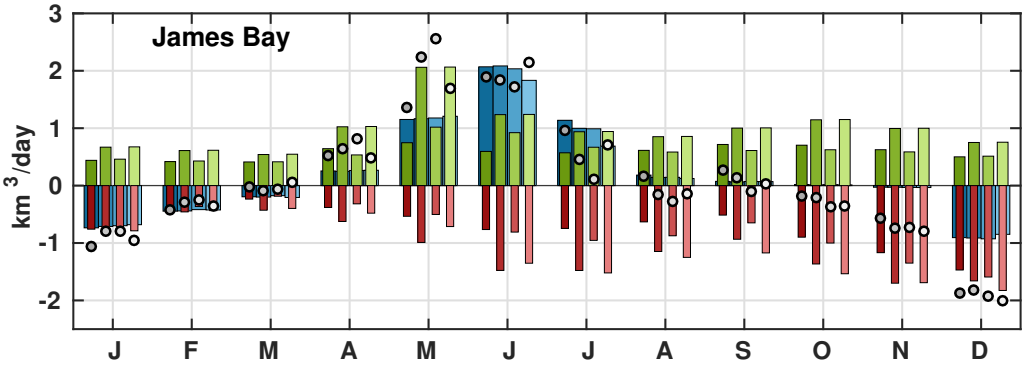

(e)

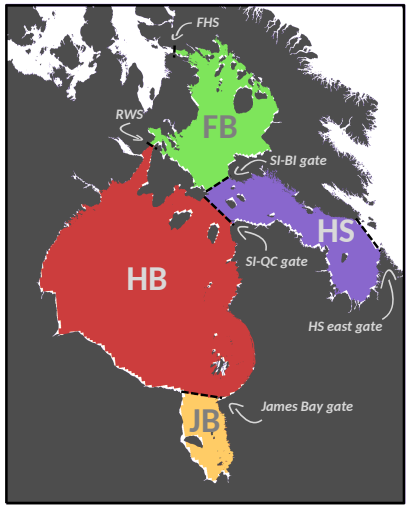

(f)

Figure 13 (Cont.): Gates are indicated in (d) with back dashed lines. Abbreviations for each gate are as follows: FHS for Fury and Hecla Strait, RWS for Roes Welcome Sound, SI-BI gate for Southampton Island-Baffin Island gate, SI-QC gate for Southampton Island-Quebec gate, and HS east gate for Hudson Strait east gate.

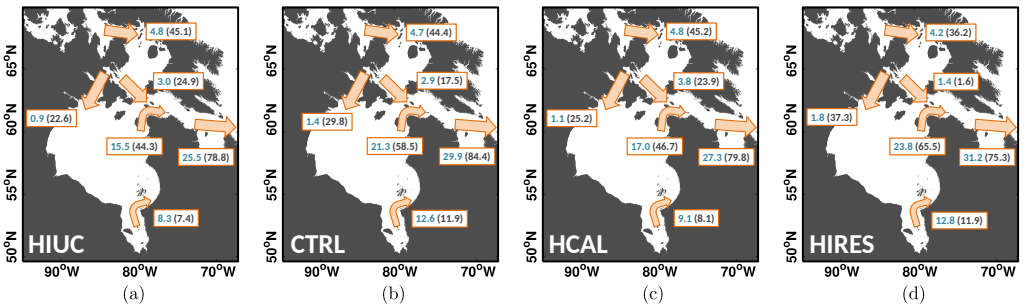

(a) (b) (c) (d)

Figure 14: Advected freshwater (volume) fluxes shown in blue (black) between basins in the HBC for four experiments, (a) HIUC, (b) CTRL, (c) HCAL, and (d) HIRES. Fluxes are averaged from 2004–2016, with units of mSv (1 mSv = 1000 m^3/s).

Figure 13 (lightest shaded symbols) shows the freshwater seasonal cycle for all regions of the HBC for the HIRES simulation . The freshwater seasonal cycle of both the HBC, as a whole, Hudson Bay proper, and Foxe Basin are not largely impacted by increased resolution. Differences between experiments are more clearly seen in Hudson Strait (Figure 13d) and James Bay (Figure 13e). Advection into and out of Hudson Strait is generally smaller in all months (for the exception of January and February), with little advection in December, while net freshwater import occurs in December in CTRL. James Bay freshwater advection is also diminished during the first part of the year, with increasing advection occurring in May/June and maximum summertime advection occurring in July, while CTRL has maintained peak advection through June and July. Advection is larger throughout the fall in HIRES compared to CTRL.

HIRES experiment fluxes between each region of the HBC are shown in Figure 14d. Freshwater and volume fluxes from James Bay are similar between CTRL and HIRES, and lower through Fury and Hecla Strait. Lower

freshwater fluxes occur between Foxe Basin and Hudson Strait, with volume fluxes being largely reduced in HIRES to only 1.6 mSv compared to 17.5 mSv in CTRL. Fluxes through Roes Welcome Sound and between Southampton Island and Quebec are larger in HIRES than CTRL, in addition to higher freshwater fluxes out of Hudson Strait into the North Atlantic. Volume fluxes, however, were smaller than CTRL out of Hudson Strait.

3.3. Boundary–Interior exchange in Hudson Bay

Using the annual mean barotropic streamfunction to determine the boundary between the interior and boundary regions of Hudson Bay, we investigated processes involved in freshwater exchange between the two regions. We chose the annual mean -0.18 Sv (1 Sv = 10^6 m^3/s) contour (Figure 15, top panels) for our analysis, as this was the largest value which was a closed contour in Hudson Bay in the HIRES simulation. The total freshwater and volume transport, in addition to the Ekman, turbulent, and mean flow contributions are shown in Figure 15 for the four experiments. Ekman transports were calculated using:

$$T_{EKy} = \frac{-1}{f\rho}\tau_x dx \tag{4}$$

$$T_{EKx} = \frac{1}{f\rho}\tau_y dy \tag{5}$$

where T_{EKx} and T_{EKy} are the Ekman transports in the model grid x and y directions respectively. Grid cell width is denoted by dx and dy in the x and y directions respectively, f the Coriolis parameter, and ρ represents density. Surface stress in the model grid x and y directions is given by τ_x and τ_y respectively. The freshwater transport due to Ekman transport is calculated by multiplying the Ekman volume transport with the freshwater

concentration in the top 24 m (Yang, 2006). The total flow ($\boldsymbol{v}$) can be decomposed into the mean and turbulent components. Here we assume the 5-day average model output as the total flow ($\boldsymbol{v}$) and a running 25 day mean as the mean flow component ($\bar{\boldsymbol{v}}$). Thus the turbulent component is given by $\boldsymbol{v}' = \boldsymbol{v} - \bar{\boldsymbol{v}}$.

On average, we see minimal turbulent freshwater exchange between the boundary and interior (Figure 15, orange), while the mean component of the flow (yellow) contributes to the majority of freshwater exchanged, with significant contributions from Ekman transport (purple). It should be noted that both the turbulent and Ekman components of the flow are highly variable, but the variability has been averaged out in the mean seasonal cycle. Ekman transport through time (not shown) reach magnitudes of 10 km^3/day, with the largest values occurring between September–December. Turbulent fluxes have smaller magnitudes, reaching over 6 km^3/day in fall, and have lower values during winter months (January–April) with a maximum value of almost 3 km^3/day (not shown).

Net freshwater advection (Figure 15, blue) is directed out of the interior in all experiments. Comparing the HIUC and CTRL experiments (Figures 15e and 15f), about three times more freshwater is exported out of the interior from January–April than CTRL, in addition to peak export in October being larger as well (blue). Peak import in July is similar in both experiments. The total freshwater flux is mostly determined by the mean component of the flow, having a comparable seasonal cycle. The mean flow in summer has been shown to have anticyclonic flow in eastern Hudson Bay, generated by the spring freshet and reinforced by the mean wind patterns, causing

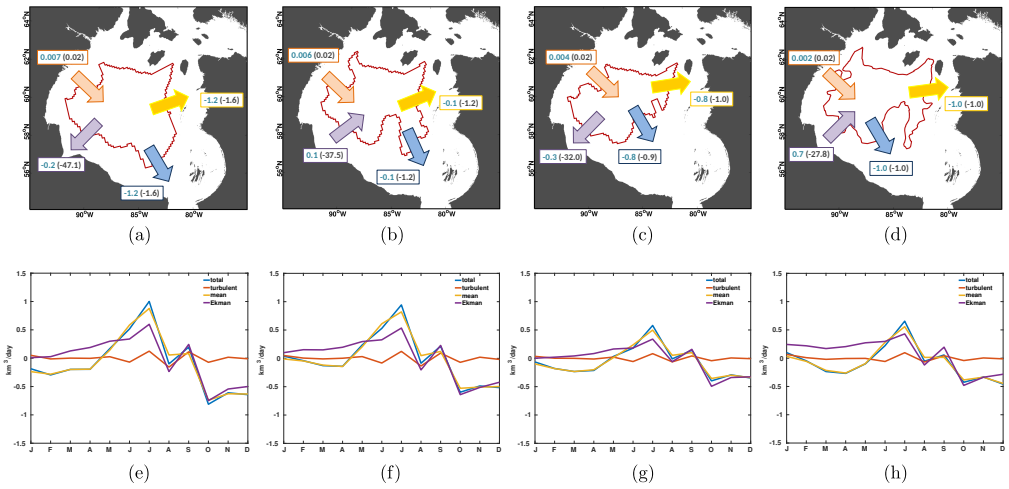

Figure 15: Freshwater exchange between Hudson Bay interior and boundary. Annual mean transports (top panels) of mean freshwater (volume) exchange in blue (black), in units of mSv, across the mean barotropic streamfunction (-0.18 Sv contour, red line), and the seasonal cycle of each process (bottom panels, units of km^3/day) are shown for four model experiments, (a,e) HIUC, (b,f) CTRL, (c,g) HCAL, and (d,h) HIRES. Blue represents the total freshwater exchange between the two regions, while yellow, orange, and purple show the mean, turbulent, and Ekman components of the flow respectively. Note that the arrows show the direction of the freshwater flux, with the associated magnitude, while the arrow locations are arbitrary.

freshwater to enter the interior as indicated by Gough et al. (2005). The net and mean component volume flux is directed out of the interior and is similar in magnitude for both experiments. The turbulent component of the flow is also similar for both volume and freshwater transports for the two experiments. Ekman volume transport in both experiments is directed out of the interior, with HIUC having more water directed out of the interior on average than CTRL. Ekman freshwater transport is a source to the interior in CTRL, while it is a sink in the HIUC experiment. This can be explained by more freshwater entering the interior with the DT runoff at the beginning of the year compared to the HIUC discharge, along with weaker freshwater export in the second half of the year (Figure 15).

The HCAL experiment (Figures 15c and 15g) is different from the other two ¼° experiments as the annual mean -0.18 Sv streamline is not present in southeastern Hudson Bay. This results in weaker exchange between the boundary and the interior compared to both HIUC and CTRL, and is most similar to the HIRES interior-boundary exchange. The turbulent component of the flow in HCAL is a net source of both volume and freshwater to the interior while Ekman transport is a net sink of freshwater and volume. Ekman transport is still a source of freshwater in summer and a sink in fall, however magnitudes of the annual cycle are reduced. Similarly for both the mean and total freshwater transports, magnitudes are weaker in both summer and fall in HCAL compared to HIUC and CTRL.

Figures 15d and 15h show freshwater exchange between the interior and boundary regions of Hudson Bay for the HIRES run. The annual mean barotropic streamfunction has a more convoluted shape in the ⅟₁₂° than the

¼° experiments. The freshwater exchange between the interior and boundary is still dominated by the mean component of the flow (yellow), but with a diminished seasonal cycle. We see larger magnitudes of freshwater export out of the interior in late winter/early spring, which leads to larger net export values on average in HIRES than CTRL, for both the mean and total freshwater exchange components. Ekman volume transport is directed out of the interior on average, however, Ekman freshwater transport is directed into the interior on average in the HIRES experiment (Figure 15d), as with CTRL, but with a larger magnitude. Ekman transport of freshwater into the interior is maintained for the first seven months of the year, while in CTRL, import of freshwater over the first three months is less than HIRES (Figure 15f and 15h). The turbulent component of the flow is small in both experiments, but more significant on shorter time scales. This, however, is beyond the scope of this study.

Freshwater flowing from the interior to the boundary, instead of from the boundary to the interior, may seem counter intuitive, since runoff flows directly into the boundary. In this analysis, we do not include the lateral movement of sea ice in our freshwater exchanges between the two regions. Therefore, sea ice imported to the interior is solid freshwater, and is only included in the lateral fluxes if the sea ice melts and the resulting liquid freshwater is transported across the streamline. Another source of freshwater export from the interior is if water more saline than the reference value leaves the boundary and crosses the streamline, which results in a freshwater flux out of the interior to the boundary.

There are still open questions with regards to the retention of freshwater

in the bay. Is the bay opposite to the Beaufort Gyre, with a predominantly cyclonic flow with freshwater retention events? This topic requires further study, as this might provide some key insights to processes occurring in the bay and the resulting freshwater fluxes to the North Atlantic.

3.4. HBC Residence Time

We used the Lagrangian tool, Ariane, to track river discharge entering the HBC at the coastlines to estimate the residence time for this region. We use the CTRL simulation only for this analysis. Figure 16 shows the percentage of Ariane particles remaining in the HBC (Figure 16a), and the particle depth distribution at the end of December 2016 for each of the four regions (Figure 16b). After being released 13 years earlier, 16.6% of particles released in Hudson Bay remain in the HBC. The majority of particles are in the top 60 m, while a few particles reach depths of 200 m and below. Particles that remain are fairly well distributed around Hudson and James Bays, as well as along the southern coast of Hudson Strait. Hudson Bay particles do enter Foxe Basin, and for the most part, remain in the south, near Southampton Island, with few being located farther north.

The majority of particles released in James Bay leave the HBC after 4 years, with a slow decline to 14.2% in the following 9 years (Figure 16a). As with Hudson Bay, the highest concentration of particles are within the top 60 m. Remaining James Bay particles are found to be well distributed in Hudson Bay and in the Hudson Strait outflow. Once again, particles that reach Foxe Basin, are mostly in the south, at varying depths, ranging from the surface to almost 300 m.

The region with the most particles remaining in the HBC is Foxe Basin, at

38.7% (Figure 16a). Foxe Basin particles are well distributed throughout the HBC, and has a smoother depth profile than the other HBC regions. Foxe Basin particles are mixed to deeper depths north of Southampton Island, likely due to the many polynyas in the region (Prinsenberg, 1986a). Particles are more concentrated in eastern Foxe Basin and likely were released in the vicinity, where they have remained.

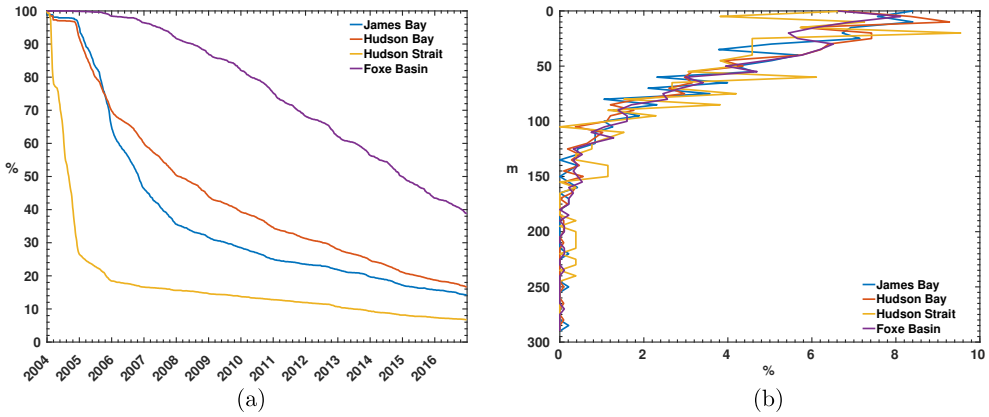

Figure 16: Particles released using Ariane and tracked for 13 years. The time series of particles remaining in the HBC (left) and final particle depth distribution of remaining particles in the HBC (right) for each of the four regions.

Fitting a trend line to the time series of the number of particles remaining in the HBC, we can estimate the residence time for particles released in each region. Using a 10% threshold, we found that particles released in Hudson Bay, using an exponential curve, can remain in the HBC for 17.6 years. While Foxe Basin has a residence time of 18.7 years using a linear polynomial trend line. Hudson Strait has the shortest residence time of 9.5 years (no trend line used). Finally, James Bay was estimated to have a residence time of 21.5 years using an exponential curve. We suggest a topic of future

work would be to investigate the temporal and spatial variability of residence times. Particles released during the spring freshet may have shorter residence times than those released in winter, while particles released in northwestern Hudson Bay likely have a longer residence time than those released along the eastern coast.

4. Discussion

In this study we investigated the sensitivity of freshwater in the HBC to model resolution and runoff forcing. This sensitivity analysis is necessary for understanding the role of model resolution and runoff forcing on the freshwater budget and indicates regions where small scale processes and river discharge are important. To our knowledge, there has been no investigation on HBC freshwater sensitivity to model resolution or runoff forcing. This study allows us to see the sensitivity of the region to various river discharge datasets in addition to the impacts of model resolution, and will assist in understanding differences between modelling studies. The results obtained here also have implications for pathways and residence times of various nutrients or pollutants commonly found in river discharge.

Our estimates of surface fluxes are comparable to some of the early estimates done by Prinsenberg (1988), with larger peak freshwater fluxes in the summer of 18 km^3/day compared to their 12 km^3/day (including areas of both Hudson Bay and James Bay). Minimum surface fluxes are similar in both studies, around -10 km^3/day. Hudson and James Bay surface fluxes calculated by St-Laurent et al. (2011) are roughly 8-23% (13–42 km^3/yr) lower than the experiments in this study. Mean Hudson and James Bay

runoff shown here accounts for 37%–41% (510–756 km^3/yr) of the freshwater budget, while average runoff in St-Laurent et al. (2011) accounts for 41% (607 km^3/yr) of the freshwater budget for the same region. Additionally, in their modelling study, total freshwater advection out of the Hudson and James Bay area was 50% of the freshwater budget (743 km^3/yr), while our estimates are lower, ranging from 32%–38% (460–692 km^3/yr).

Earlier estimates of freshwater and volume fluxes through Fury and Hecla Strait vary, with winter volume fluxes of 40 mSv (Barber, 1965), and summer volume fluxes of 100 mSv (Sadler, 1982), with corresponding freshwater fluxes of 1.2 and 3.0 mSv respectively. Using the aforementioned volume fluxes, Straneo and Saucier (2008b) estimated the year round volume and freshwater fluxes to be 70 and 2.8 mSv (S_{ref}=33) respectively. The volume fluxes obtained here, are closest to the winter season fluxes from Barber (1965), ranging from 36.2–45.2 mSv, with freshwater fluxes being larger than previous estimates with 4.2–4.8 mSv. Our larger freshwater flux estimates are partly due to the fact that Fury and Hecla Strait is wider in the model domain than in reality due to the model resolution, while previous assumptions, such as constant salinity and volume transport for consecutive months of the year, might also lead to discrepancies between studies.

Hudson Strait net volume and freshwater fluxes were estimated by Straneo and Saucier (2008b) to be 101 and 35 mSv respectively, while Saucier et al. (2004) stated that the freshwater flux relative to a reference salinity of 34.8 should be 29 mSv. Drinkwater (1988) also states that the net outflow of Hudson Strait should be about 100 mSv, the combined contribution of river discharge and flow through Fury and Hecla Strait. The net freshwater

and volume fluxes simulated here range from 25.5–31.2 and 75.3–84.4 mSv respectively. Both sets of values are smaller than those stated by Straneo and Saucier (2008b). However if we use a similar assumption to Straneo and Saucier (2008a), that all inflow through Hudson Strait has a mean salinity of 33, and does not contribute to the freshwater flux, our range of 25.5–31.2 mSv fits with the estimate of 27–28 mSv from Straneo and Saucier (2008a). Additionally, Straneo and Saucier (2008a) estimate the volume outflow of Hudson Strait to be between 1–1.2 Sv, whereas in this suite of experiments, we have a volume outflow range of 1.2–1.4 Sv.

Fluxes through Roes Welcome Sound and the three eastern gates connecting Hudson Bay and Hudson Strait were modelled by St-Laurent et al. (2011). They found freshwater and volume fluxes through Roes Welcome Sound to be 0.5 and 18 mSv respectively, both of which are lower than the fluxes simulated here, with freshwater fluxes ranging from 0.9–1.8 mSv, and volume fluxes in the range of 22.6–37.3 mSv. We find that our range for freshwater fluxes through the passage between Southampton Island and Quebec of 15.5–23.8 mSv, are lower than or comparable to the St-Laurent et al. (2011) value of 24 mSv, with the HIRES experiment having the best agreement. Volume fluxes obtained here are in the range of 44.3–65.5 mSv, compared to the volume flux of 35 mSv found by St-Laurent et al. (2011).

The volume fluxes through the Southampton–Baffin Island gate in this study range from 1.6–24.9 mSv out of Foxe Basin. These values are lower than the modelling study done by Defossez et al. (2012), who found a net volume flux of 56 mSv out of Foxe Basin, with outflow from the basin at both the surface and at depth, and inflow at intermediate depths for both

summer and winter. A positive–negative estuarine circulation in the gate was indicated, with salt gain (loss) in winter (summer) at the surface, while at depth, salt loss occurred in both summer and winter (Defossez et al., 2012). One explanation for this discrepancy between the two studies is the horizontal and vertical resolution, where HIUC, HCAL, and CTRL have a slightly coarser resolution in this region, while the HIRES experiment has twice the resolution. The vertical resolution used here is higher at the surface compared to Defossez et al. (2012), however coarser at depth. Additionally, this study uses 5-day averages for 13 years, while Defossez et al. (2012) uses 3-hour averages over a 4 year time period.

The freshwater exchange between the Hudson Bay boundary and interior has been studied previously by St-Laurent et al. (2011, 2012). In this study, the barotropic streamfunctions consider the whole water column over 13 years, causing them to be smaller than those in St-Laurent et al. (2011). Nonetheless, our results also show that freshwater from the boundary is transported to the interior in summer via Ekman transport, and vice versa in the fall. They neglected the eddy and mean components of the flow and assumed the flow could be separated into the geostrophic and Ekman components. Our 5-day mean Ekman fluxes agree in magnitude with those modelled by St-Laurent et al. (2011). Our turbulent component of the flow, however, has fluxes into the interior up to 6 km^3/day, and thus cannot be ignored on shorter time scales. Though, investigating the specifics of the turbulent component is beyond the scope of this study.

St-Laurent et al. (2012) used a conceptual model (1979–2007) and found turbulent fluxes were low, but were a freshwater source to the interior, in

agreement with our mean turbulent flow value. Ekman transport led to net export of freshwater out of the interior throughout the whole year, which disagrees with our results, as we have freshwater import into the interior from January–July, and freshwater export from October–December. Additionally, net Ekman freshwater transport is out of the interior in the HIUC and HCAL experiments, but in the experiments using DT runoff, net Ekman freshwater transport is a freshwater source to the interior. Ekman transport is not the only process transporting freshwater to the interior in summer, however, the mean component of the flow, which includes the contributions of Ekman tranport, also exchanges freshwater between the two regions. This component of the flow can be explained by the summer flow pattern, whereby the sea surface height increases during summer, induces westward flow along the southern coast of Hudson Bay that is deflected northwards, generating anticyclonic flow in eastern Hudson Bay.

Regarding residence time of river discharge, our results indicate that the residence time for the HBC could be as long as 21.5 years. Previous estimates of residence time were based on salinity profiles and distribution, such as Prinsenberg (1984, 1986b) who found a residence time of 6.6 years. Ingram and Prinsenberg (1998) state that the result obtained by Prinsenberg (1984, 1986b) is actually the estuary residence time, which only considers freshwater from river discharge not sea ice melt. A residence time of 1–2 years was estimated by Ingram and Prinsenberg (1998) based on the results of Prinsenberg (1984) but with the inclusion of sea ice melt in the calculation. In the modelling study conducted by St-Laurent et al. (2011), a tracer was used to evaluate the transit time of river discharge in Hudson Bay, which

they found was 3 years on average. However, Pett et al. (1982) estimated the residence time of deep water in Hudson Bay to be in the range of 4–14 years, with the use of apparent oxygen utilisation measurements, which is the difference between observed dissolved oxygen concentration and the equilibrium saturated oxygen concentration for those water properties. With the use of $\delta^{18}O$ as a freshwater tracer in Hudson Bay, Granskog et al. (2011) found river water at depth in Hudson Bay, which is consistent with the long residence time estimated by Pett et al. (1982). Granskog et al. (2011) suggest that 6–16% of Hudson and James Bay yearly river discharge is mixed into deeper waters. Our estimates of the Hudson Bay and James Bay residence time of 17.6 and 21.5 years respectively, compare well with the longer residence time estimate of Pett et al. (1982). Even though a full investigation of river runoff pathways is beyond the scope of this paper, it brings up interesting questions as to the processes involved, such as those mentioned by Granskog et al. (2011), and runoff pathways from different regions in the HBC.

Our study has provided a look at present day freshwater dynamics in the HBC, in addition to evaluating the sensitivity of the region to model resolution and runoff forcing. Using different estimates of runoff allows us to test the sensitivity of the region, which has importance for future studies. Our main findings in this paper are:

Sensitivity to runoff Overall, the seasonality of freshwater is robust, however the strength and magnitude of fluxes were impacted. Increased discharge in runoff datasets lead to stronger circulation patterns, while decreased discharge and seasonality throughout the year lead to weaker circulation. Lower freshwater and volume exchange between subregions

and between the HBC and North Atlantic were also due to decreased discharge and seasonality.

Sensitivity to model resolution Increased model resolution was able to reproduce freshwater contained in sea ice, however there was generally little impact on fluxes through gates with simple flow dynamics. Small scale processes were found to be important through Southampton–Baffin Island Gate. Freshwater interior-boundary exchange was also impacted by higher model resolution via the Ekman and mean components of the flow.

HBC residence time Particles released along the coast indicate that the residence time for the HBC is as long as 21.5 years, with HBC residence times for Foxe Basin, Hudson Bay, James Bay, and Hudson Strait being 18.7, 17.6, 21.5, and 9.5 years respectively, agreeing with previous estimates.

Our work highlights topics for future work such as the role of the turbulent component of the flow and freshwater retention in Hudson Bay. A complete understanding of the pathways of river discharge, in addition to regional variability of residence time, is important for tracing various nutrients in addition to pollutants, such as mercury (Hare et al., 2010; Wang and Zhang, 2013), both of which can impact the ecosystem and food sources for communities in the HBC.

Acknowledgements

We would like to thank Environment and Climate Change Canada for the use of the CGRF forcing fields, as well as the producers of GLORYS for the reanalysis data that we use to initialize our model simulations as well as providing our model with open boundary conditions. Thank you to Dr. Gregory Smith who provided the CGRF atmospheric forcing to force our ocean model. This work is part of the BaySys project, thus we thank the Natural Sciences and Engineering Research Council of Canada and Manitoba Hydro for funding the BaySys project (CRDPJ 470028-14). We are grateful for the use of the HYPE dataset which was provided by BaySys Team 2 (Matt MacDonald, Tricia Stadnyk, and Stephen Déry). We are grateful to Dr. J Bamber for the Greenland melt dataset, and to Aviso, ArcticNet, ICES, and MEDS for their observational data which was used to evaluate the model simulations. Observational datasets such as SST data from NOAA ESRL/PSD, ice drift from EUMETSAT OSISAF, and ice concentration and thickness data from Integrated Climate Data Centre at the University of Hamburg were also greatly appreciated for model evaluation. Computational resources used for our work were provided by Westgrid and Compute Canada, which made this work possible.

References

Aagaard, K., Carmack, E.C., 1989. The role of sea ice and other fresh water in the Arctic circulation. Journal of Geophysical Research: Oceans 94, 14485–14498. doi:10.1029/JC094iC10p14485.

Andersson, J.C.M., Pechlivanidis, I.G., Gustafsson, D., Donnelly, C., Arheimer, B., 2013. Key factors for improving large-scale hydrological model performance, in: Lekkas, T. (Ed.), Proceedings of the 13th International Conference on Environmental Science and Technology, Univ Aegean; Global Network Environm Sci & Technol. Global Nest, Secritariat, Univ, Aegean, 30, Voulgaroktonou Str, Athens, GR 114 72, Greece. pp. 77–88. 13th International Conference on Environmental Science and Technology (CEST), Athens, Greece, Sep 05-07, 2013.

Bamber, J., van den Broeke, M., Ettema, J., Lenaerts, J., Rignot, E., 2012. Recent large increases in freshwater fluxes from Greenland into the North Atlantic. Geophysical Research Letters 39. doi:10.1029/2012GL052552.

Barber, F.G., 1965. Current Observations in Fury and Hecla Strait. Journal of the Fisheries Research Board of Canada 22, 225–229. doi:10.1139/f65-021.

Blanke, B., Arhan, M., Madec, G., Roche, S., 1999. Warm Water Paths in the Equatorial Atlantic as Diagnosed with a General Circulation Model. Journal of Physical Oceanography 29, 2753–2768. doi:10.1175/1520-0485(1999)029<2753:WWPITE>2.0.CO;2.

Blanke, B., Delecluse, P., 1993. Variability of the Tropical Atlantic Ocean Simulated by a General Circulation Model with Two Different Mixed-Layer Physics. Journal of Physical Oceanography 23, 1363–1388. doi:10.1175/1520-0485(1993)023<1363:VOTTAO>2.0.CO;2.

Blanke, B., Raynaud, S., 1997. Kinematics of the Pacific Equatorial

Undercurrent: An Eulerian and Lagrangian Approach from GCM Results. Journal of Physical Oceanography 27, 1038–1053. doi:10.1175/1520-0485(1997)027<1038:KOTPEU>2.0.CO;2.

de Boisséson, E., Thierry, V., Mercier, H., Caniaux, G., Desbruyères, D., 2012. Origin, formation and variability of the Subpolar Mode Water located over the Reykjanes Ridge. Journal of Geophysical Research: Oceans 117. doi:10.1029/2011JC007519.

Bougeault, P., Lacarrere, P., 1989. Parameterization of orography-induced turbulence in a mesobeta-scale model. Monthly Weather Review 117, 1872 – 1890.

Castro de la Guardia, L., Myers, P.G., Derocher, A.E., Lunn, N.J., Terwisscha van Scheltinga, A.D., 2017. Sea ice cycle in western Hudson Bay, Canada, from a polar bear perspective. Marine Ecology Progress Series 564, 225–233.

Dai, A., Qian, T., Trenberth, K.E., Milliman, J.D., 2009. Changes in Continental Freshwater Discharge from 1948 to 2004. Journal of Climate 22, 2773–2792. doi:10.1175/2008JCLI2592.1.

Dai, A., Trenberth, K.E., 2002. Estimates of Freshwater Discharge from Continents: Latitudinal and Seasonal Variations. Journal of Hydrometeorology 3, 660–687. doi:10.1175/1525-7541(2002)003<0660:EOFDFC>2.0.CO;2.

Defossez, M., Saucier, F., Myers, P., Caya, D., Dumais, J., 2012. Comparing Winter and Summer Simulated Estuarine Circulations in Foxe Basin, Canada. Atmosphere-Ocean 50, 386 – 401.

Déry, S., T.A., S., M., M., Koenig, K., C., G., 2018. Flow regulation transcends daily natural variation in Hudson Bay's two largest rivers. Hydrol. Process Accepted.

Déry, S.J., Stieglitz, M., McKenna, E.C., 2005. Characteristics and Trends of River Discharge into Hudson, James, and Ungava Bays, 1964–2000. Journal of Climate 18, 2540–2557.

Déry, S.J., Wood, E.F., 2004. Teleconnection between the Arctic Oscillation and Hudson Bay river discharge. Geophysical Research Letters 31. doi:10.1029/2004GL020729.

Drinkwater, K.F., 1988. On the Mean and Tidal Currents in Hudson Strait. Atmosphere–Ocean 26, 252 – 266.

Déry, S.J., Hernández-Henríquez, M.A., Burford, J.E., Wood, E.F., 2009. Observational evidence of an intensifying hydrological cycle in northern Canada. Geophysical Research Letters 36. doi:10.1029/2009GL038852.

Déry, S.J., Mlynowski, T.J., Hernández-Henríquez, M.A., Straneo, F., 2011. Interannual variability and interdecadal trends in Hudson Bay streamflow. Journal of Marine Systems 88, 341 – 351.

Déry, S.J., Stadnyk, T.A., MacDonald, M.K., Gauli-Sharma, B., 2016. Recent trends and variability in river discharge across northern Canada. Hydrology and Earth System Sciences 20, 4801 – 4818.

Dukhovskoy, D.S., Myers, P.G., Platov, G., Timmermans, M.L., Curry, B., Proshutinsky, A., Bamber, J.L., Chassignet, E., Hu, X., Lee, C.M., Somavilla, R., 2016. Greenland freshwater pathways in the sub-Arctic seas from

model experiments with passive tracers. Journal of Geophysical Research: Oceans 121, 877–907. doi:10.1002/2015JC011290.

Fichefet, T., Maqueda, M.A.M., 1997. Sensitivity of a global sea ice model to the treatment of ice thermodynamics and dynamics. Journal of Geophysical Research: Oceans 102, 12609–12646. doi:10.1029/97JC00480.

Gagnon, A.S., Gough, W.A., 2002. Hydro-Climatic trends in the Hudson Bay Region, Canada. Canadian Water Resources Journal / Revue canadienne des ressources hydriques 27, 245–262. doi:10.4296/cwrj2703245.

Gagnon, A.S., Gough, W.A., 2005. Trends in the Dates of Ice Freeze-up and Breakup over Hudson Bay, Canada. Arctic 58, 370–382.

Gaspar, P., Gregoris, Y., Lefevre, J., 1990. A simple eddy kinetic-energy model for simulations of the oceanic vertical mixing - Tests at station Papa and long-term upper ocean study site. Journal of Geophysical Research: Oceans 95, 16179 – 16193.

Gelfan, A., Gustafsson, D., Motovilov, Y., Arheimer, B., Kalugin, A., Krylenko, I., Lavrenov, A., 2017. Climate change impact on the water regime of two great Arctic rivers: modeling and uncertainty issues. Climatic Change 141, 499–515. doi:10.1007/s10584-016-1710-5.

Gillard, L.C., Hu, X., Myers, P.G., Bamber, J.L., 2016. Meltwater pathways from marine terminating glaciers of the Greenland ice sheet. Geophysical Research Letters 43, 10,873–10,882. doi:10.1002/2016GL070969.

Gough, W., Cornwell, A., Tsuji, L., 2004a. Trends in Seasonal Sea Ice Duration in Southwestern Hudson Bay. Arctic 57, 299–305. doi:10.14430/arctic507.

Gough, W.A., Gagnon, A.S., Lau, H.P., 2004b. Interannual Variability of Hudson Bay Ice Thickness. Polar Geography 28, 222–238. doi:10.1080/789610188.

Gough, W.A., Robinson, C., Hosseinian, R., 2005. The Influence of James Bay River Discharge on Churchill, Manitoba Sea Level. Polar Geography 29, 213–223. doi:10.1080/789610202.

Granskog, M.A., Kuzyk, Z.Z.A., Azetsu-Scott, K., Macdonald, R.W., 2011. Distributions of runoff, sea-ice melt and brine using δ^{18}O and salinity data — A new view on freshwater cycling in Hudson Bay. Journal of Marine Systems 88, 362 – 374.

Granskog, M.A., Macdonald, R.W., Mundy, C.J., Barber, D.G., 2007. Distribution, characteristics and potential impacts of chromophoric dissolved organic matter (CDOM) in Hudson Strait and Hudson Bay, Canada. Continental Shelf Research 27, 2032 – 2050.

Castro de la Guardia, L., Derocher, A.E., Myers, P.G., Terwisscha van Scheltinga, A.D., Lunn, N.J., 2013. Future sea ice conditions in Western Hudson Bay and consequences for polar bears in the 21st century. Global Change Biology 19, 2675–2687. doi:10.1111/gcb.12272.

Hare, A.A., Stern, G.A., Kuzyk, Z.Z.A., Macdonald, R.W., Johannessen, S.C., Wang, F., 2010. Natural and Anthropogenic Mercury Distribution

in Marine Sediments from Hudson Bay, Canada. Environmental Science & Technology 44, 5805–5811. doi:10.1021/es100724y.

Hochheim, K.P., Barber, D.G., 2010. Atmospheric forcing of sea ice in Hudson Bay during the fall period, 1980–2005. Journal of Geophysical Research: Oceans 115. doi:10.1029/2009JC005334.

Hochheim, K.P., Barber, D.G., 2014. An Update on the Ice Climatology of the Hudson Bay System. Arctic, Antarctic, and Alpine Research 46, 66–83. doi:10.1657/1938-4246-46.1.66.

Holdsworth, A.M., Myers, P.G., 2015. The Influence of High-Frequency Atmospheric Forcing on the Circulation and Deep Convection of the Labrador Sea. Journal of Climate 28, 4980–4996. doi:10.1175/JCLI-D-14-00564.1.

Holmes, R.M., McClelland, J.W., Peterson, B.J., Tank, S.E., Bulygina, E., Eglinton, T.I., Gordeev, V.V., Gurtovaya, T.Y., Raymond, P.A., Repeta, D.J., Staples, R., Striegl, R.G., Zhulidov, A.V., Zimov, S.A., 2012. Seasonal and Annual Fluxes of Nutrients and Organic Matter from Large Rivers to the Arctic Ocean and Surrounding Seas. Estuaries and Coasts 35, 369–382. doi:10.1007/s12237-011-9386-6.

Hu, X., Myers, P.G., 2013. A Lagrangian view of Pacific water inflow pathways in the Arctic Ocean during model spin-up. Ocean Modelling 71, 66 – 80. doi:10.1016/j.ocemod.2013.06.007.

Hu, X., Sun, J., Chan, T.O., Myers, P.G., 2018. Thermodynamic and dynamic ice thickness contributions in the Canadian Arctic Archipelago

in NEMO-LIM2 numerical simulations. The Cryosphere 12, 1233–1247. doi:10.5194/tc-12-1233-2018.

Hunke, E.C., Dukowicz, J.K., 1997. An Elastic–Viscous–Plastic Model for Sea Ice Dynamics. Journal of Physical Oceanography 27, 1849–1867. doi:10.1175/1520-0485(1997)027<1849:AEVPMF>2.0.CO;2.

Ingram, R.G., Prinsenberg, S., 1998. Coastal Oceanography of Hudson Bay and Surrounding Eastern Canadian Arctic Waters Coastal Segment, in: Robinson, A.R., Brink, K.H. (Eds.), The Sea. John Wiley and Sons, Toronto. volume 11. chapter 5, pp. 835–861.

Kowal, S., Gough, W.A., Butler, K., 2017. Temporal evolution of Hudson Bay Sea Ice (1971–2011). Theoretical and Applied Climatology 127, 753–760. doi:10.1007/s00704-015-1666-9.

Landy, J.C., Ehn, J.K., Babb, D.G., Thériault, N., Barber, D.G., 2017. Sea ice thickness in the Eastern Canadian Arctic: Hudson Bay Complex & Baffin Bay. Remote Sensing of Environment 200, 281 – 294. doi:10.1016/j.rse.2017.08.019.

Large, W., Yeager, S., 2004. Diurnal to Decadal Global Forcing For Ocean and Sea-Ice Models: The Data Sets and Flux Climatologies. NCAR/TN-460+STR NCAR Technical Note. National Center for Atmospheric Research.

Lavergne, T., Eastwood, S., Teffah, Z., Schyberg, H., Breivik, L.A., 2015. Sea ice motion from low-resolution satellite sensors: An alternative method and

its validation in the Arctic. Journal of Geophysical Research: Oceans 115. doi:10.1029/2009JC005958.

Lazier, J., Hendry, R., Clarke, A., Yashayaev, I., Rhines, P., 2002. Convection and restratification in the Labrador Sea, 1990–2000. Deep Sea Research Part I: Oceanographic Research Papers 49, 1819 – 1835. doi:10.1016/S0967-0637(02)00064-X.

Lindström, G., Pers, C., Rosberg, J., Strömqvist, J., Arheimer, B., 2010. Development and testing of the HYPE (Hydrological Predictions for the Environment) water quality model for different spatial scales. Hydrology Research 41, 295–319. doi:10.2166/nh.2010.007.

Lique, C., Treguier, A.M., Blanke, B., Grima, N., 2010. On the origins of water masses exported along both sides of Greenland: A Lagrangian model analysis. Journal of Geophysical Research: Oceans 115. doi:10.1029/2009JC005316.

MacDonald, M.K., Stadnyk, T.A., Déry, S.J., Braun, M., Gustafsson, D., Isberg, K., Arheimer, B., 2018. Impacts of 1.5 and 2.0 °C Warming on Pan-Arctic River Discharge Into the Hudson Bay Complex Through 2070. Geophysical Research Letters 0. doi:10.1029/2018GL079147.

Madec, G., Delécluse, P., Imbard, M., Lévy, C., 1998. Opa 8.1 Ocean General Circulation Model reference manual. Note du Pole de Modélisation 11, 91p.

Madec, G., the NEMO team, 2008. NEMO ocean engine. Note du Pole de Modélisation .

Masina, S., Storto, A., Ferry, N., Valdivieso, M., Haines, K., Balmaseda, M., Zuo, H., Drevillon, M., Parent, L., 2017. An ensemble of eddy-permitting global ocean reanalyses from the MyOcean project. Climate Dynamics 49, 813–841. doi:10.1007/s00382-015-2728-5.

McClelland, J.W., Déry, S.J., Peterson, B.J., Holmes, R.M., Wood, E.F., 2006. A pan-arctic evaluation of changes in river discharge during the latter half of the 20th century. Geophysical Research Letters 33. doi:10.1029/2006GL025753.

McGovern, P., Gough, W., 2015. East-West Asymmetry in Coastal Temperatures of Hudson Bay as a Proxy for Sea Ice. Arctic 68, 445–452. doi:10.14430/arctic4522.

Müller, V., Kieke, D., Myers, P.G., Pennelly, C., Mertens, C., 2017. Temperature flux carried by individual eddies across 47°N in the Atlantic Ocean. Journal of Geophysical Research: Oceans doi:10.1002/2016JC012175.

Pett, R., Roff, J., I.P., M., 1982. Some observations and deductions concerning the deep waters of Hudson Bay. Naturaliste Canadien , 767–774.

Prinsenberg, S., 1984. Freshwater contents and heat budgets of James Bay and Hudson Bay. Continental Shelf Research 3, 191 – 200. doi:10.1016/0278-4343(84)90007-4.

Prinsenberg, S., 1986a. Chapter 12 On the Physical Oceanography of Foxe Basin, in: Martini, I. (Ed.), Canadian Inland Seas. Elsevier. volume 44 of *Elsevier Oceanography Series*, pp. 217 – 236. doi:10.1016/S0422-9894(08)70905-X.

Prinsenberg, S., 1986b. Chapter 9 Salinity and Temperature Distributions of Hudson Bay and James Bay. Elsevier Oceanography Series 44, 163 – 186. doi:10.1016/S0422-9894(08)70902-4.

Prinsenberg, S., 1988. Ice-Cover and Ice-Ridge Contributions to the Freshwater Contents of Hudson Bay and Foxe Basin. Arctic 41, 6–11. doi:10.14430/arctic1686.

Rawlins, M.A., Steele, M., Holland, M.M., Adam, J.C., Cherry, J.E., Francis, J.A., Groisman, P.Y., Hinzman, L.D., Huntington, T.G., Kane, D.L., Kimball, J.S., Kwok, R., Lammers, R.B., Lee, C.M., Lettenmaier, D.P., McDonald, K.C., Podest, E., Pundsack, J.W., Rudels, B., Serreze, M.C., Shiklomanov, A., Øystein Skagseth, Troy, T.J., Vörösmarty, C.J., Wensnahan, M., Wood, E.F., Woodgate, R., Yang, D., Zhang, K., Zhang, T., 2010. Analysis of the Arctic System for Freshwater Cycle Intensification: Observations and Expectations. Journal of Climate 23, 5715–5737. doi:10.1175/2010JCLI3421.1.

Reynolds, R.W., Smith, T.M., Liu, C., Chelton, D.B., Casey, K.S., Schlax, M.G., 2007. Daily High-Resolution-Blended Analyses for Sea Surface Temperature. Journal of Climate 20, 5473–5496. doi:10.1175/2007JCLI1824.1.

Sadler, H.E., 1982. Water flow into Foxe Basin through Fury and Hecla Strait. Naturaliste Canadien , 701 – 707.

Saucier, F., Dionne, J., 1998. A 3-D coupled ice-ocean model applied to Hudson Bay, Canada: The seasonal cycle and time-dependent climate response

to atmospheric forcing and runoff. Journal Of Geophysical Research–Oceans 103, 27689 – 27705.

Saucier, F.J., Senneville, S., Prinsenberg, S., Roy, F., Smith, G., Gachon, P., Caya, D., Laprise, R., 2004. Modelling the sea ice-ocean seasonal cycle in Hudson Bay, Foxe Basin and Hudson Strait, Canada. Climate Dynamics 23, 303 – 326.

Shiklomanov, I.A., Shiklomanov, A.I., 2003. Climatic Change and the Dynamics of River Runoff into the Arctic Ocean. Water Resources 30, 593–601. doi:10.1023/B:WARE.0000007584.73692.ca.

Smith, G.C., Roy, F., Mann, P., Dupont, F., Brasnett, B., Lemieux, J.F., Laroche, S., Bélair, S., 2014. A new atmospheric dataset for forcing ice–ocean models: Evaluation of reforecasts using the Canadian global deterministic prediction system. Quarterly Journal of the Royal Meteorological Society 140, 881–894. doi:10.1002/qj.2194.

Spreen, G., Kaleschke, L., Heygster, G., 2008. Sea ice remote sensing using AMSR-E 89-GHz channels. Journal of Geophysical Research: Oceans 113. doi:10.1029/2005JC003384. c02S03.

St-Laurent, P., Straneo, F., Barber, D.G., 2012. A conceptual model of an Arctic sea. Journal of Geophysical Research: Oceans 117. doi:10.1029/2011JC007652.

St-Laurent, P., Straneo, F., Dumais, J.F., Barber, D., 2011. What is the fate of the river waters of Hudson Bay? Journal of Marine Systems 88, 352 – 361.

Straneo, F., 2006. Heat and Freshwater Transport through the Central Labrador Sea. Journal of Physical Oceanography 36, 606–628. doi:10.1175/JPO2875.1.

Straneo, F., Saucier, F., 2008a. The outflow from Hudson Strait and its contribution to the Labrador Current. Deep-Sea Research Part I 55, 926 – 946.

Straneo, F., Saucier, F.J., 2008b. The Arctic–Subarctic Exchange Through Hudson Strait, in: Dickson, R.R., Meincke, J., Rhines, P. (Eds.), Arctic–Subarctic Ocean Fluxes: Defining the Role of the Northern Seas in Climate. Springer Netherlands, Dordrecht, pp. 249–261. doi:10.1007/978-1-4020-6774-7_11.

Tian-Kunze, X., Kaleschke, L., Maass, N., 2013. SMOS Daily Sea Ice Thickness [Nov 2010–Jan 2016]. Digital Media, ICDC, University of Hamburg, Hamburg, Germany. Updated 2016.

Wang, F., Zhang, J., 2013. Mercury contamination in aquatic ecosystems under a changing environment: Implications for the Three Gorges Reservoir. Chinese Science Bulletin 58, 141–149. doi:10.1007/s11434-012-5490-7.

Yang, J., 2006. The Seasonal Variability of the Arctic Ocean Ekman Transport and Its Role in the Mixed Layer Heat and Salt Fluxes. Journal of Climate 19, 5366–5387. doi:10.1175/JCLI3892.1.

Zhang, X., He, J., Zhang, J., Polyakov, I., Gerdes, R., Inoue, J., Wu, P., 2012. Enhanced poleward moisture transport and amplified northern high-latitude wetting trend. Nature Climate Change 3, 47 – 51.